

AD-A170 011

EXPERIMENTAL VERIFICATION OF SOLITON THEORY USING A  
MICROWAVE CROSSED-FIE. (U) UTAH UNIV SALT LAKE CITY  
DEPT OF ELECTRICAL ENGINEERING S W SHPOCK APR 86

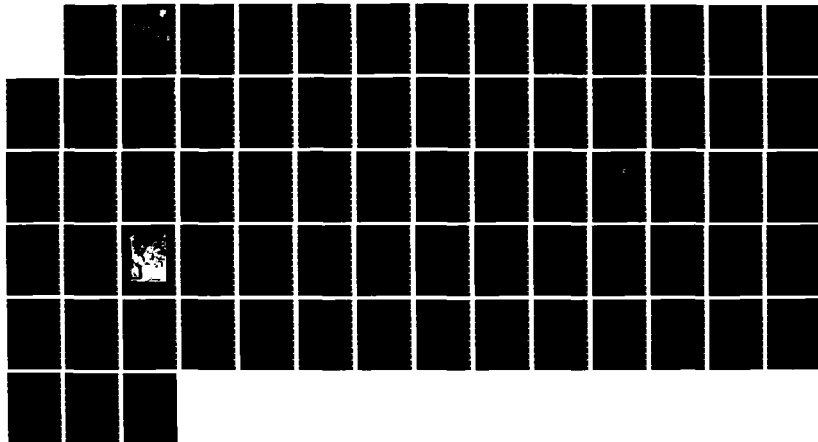
1/1

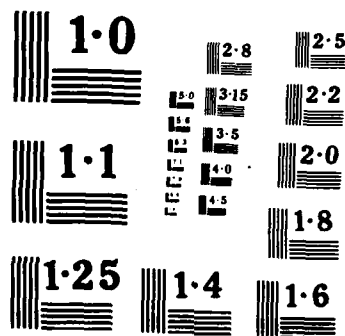
UNCLASSIFIED

RADC-TR-85-271 F30602-02-C-0161

F/G 20/3

NL





12

**RADC-TR-85-271**  
**Final Technical Report**  
**April 1986**



**AD-A170 011**

***EXPERIMENTAL VERIFICATION OF SOLITON  
THEORY USING A MICROWAVE  
CROSSED-FIELD AMPLIFIER***

**University of Utah**

**Stephen W. Shpock**

**DTIC**  
**ELECTE**  
**JUL 24 1986**  
**S D**

**APPROVED FOR PUBLIC RELEASE; DISTRIBUTION UNLIMITED**

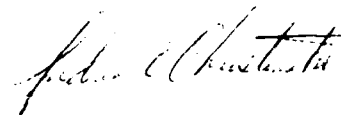
**DTIC FILE COPY**

**ROME AIR DEVELOPMENT CENTER**  
**Air Force Systems Command**  
**Griffiss Air Force Base, NY 13441-5700**

This report has been reviewed by the RADC Public Affairs Office (PA) and is releasable to the National Technical Information Service (NTIS). At NTIS it will be releasable to the general public, including foreign nations.

RADC-TR-85-271 has been reviewed and is approved for publication.

APPROVED:



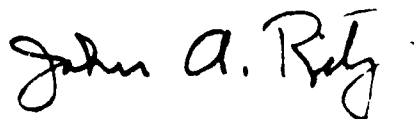
ANDREW E. CHROSTOWSKI, 1Lt, USAF  
Project Engineer

APPROVED:



FRANK J. REHM  
Technical Director  
Surveillance Division

FOR THE COMMANDER:



JOHN A. RITZ  
Plans and Programs Division

DESTRUCTION NOTICE - For classified documents, follow the procedures in DOD 5200.22-M, Industrial Security Manual, Section II-19 or DOD 5200.1-R, Information Security Program Regulation, Chapter IX. For unclassified, limited documents, destroy by any method that will prevent disclosure of contents or reconstruction of the document.

If your address has changed or if you wish to be removed from the RADC mailing list, or if the addressee is no longer employed by your organization, please notify RADC (OCTP) Griffiss AFB NY 13441-5700. This will assist us in maintaining a current mailing list.

Do not return copies of this report unless contractual obligations or notices on a specific document requires that it be returned.

UNCLASSIFIED

SECURITY CLASSIFICATION OF THIS PAGE

## REPORT DOCUMENTATION PAGE

A170 011

1a REPORT SECURITY CLASSIFICATION UNCLASSIFIED			1b RESTRICTIVE MARKINGS N/A		
2a SECURITY CLASSIFICATION AUTHORITY N/A			3 DISTRIBUTION / AVAILABILITY OF REPORT Approved for public release; distribution unlimited		
2b DECLASSIFICATION / DOWNGRADING SCHEDULE N/A					
4 PERFORMING ORGANIZATION REPORT NUMBER(S) N/A			5 MONITORING ORGANIZATION REPORT NUMBER(S) RADC-TR-85-271		
6a NAME OF PERFORMING ORGANIZATION University of Utah		6b OFFICE SYMBOL (If applicable)		7a NAME OF MONITORING ORGANIZATION Rome Air Development Center (OCTP)	
6c ADDRESS (City, State, and ZIP Code) Department of Electrical Engineering Salt Lake City UT 84112			7b ADDRESS (City, State, and ZIP Code) Griffiss AFB NY 13441-5700		
8a NAME OF FUNDING / SPONSORING ORGANIZATION AFOSR		8b OFFICE SYMBOL (If applicable) NE		9 PROCUREMENT INSTRUMENT IDENTIFICATION NUMBER F30602-82-C-0161	
8c ADDRESS (City, State, and ZIP Code) Bolling AFB Wash DC 20332			10 SOURCE OF FUNDING NUMBERS		
			PROGRAM ELEMENT NO 61102F	PROJECT NO 2305	TASK NO J9
			WORK UNIT ACCESSION NO 16		
11 TITLE (Include Security Classification) EXPERIMENTAL VERIFICATION OF SOLITON THEORY USING A MICROWAVE CROSSED-FIELD AMPLIFIER					
12 PERSONAL AUTHOR(S) Stephen W. Shpock					
13a TYPE OF REPORT Final		13b TIME COVERED FROM Sep 82 TO Sep 85		14 DATE OF REPORT (Year, Month, Day) April 1986	
15 PAGE COUNT					
16 SUPPLEMENTARY NOTATION Research accomplished in conjunction with Air Force Thermionics Engineering Research Program (AFTER)					
17 COSATI CODES			18 SUBJECT TERMS (Continue on reverse if necessary and identify by block number)		
FIELD	GROUP	SUB-GROUP	Crosed-Field Amplifier		
09	03		Soliton Analysis		
			Performance Prediction		
19 ABSTRACT (Continue on reverse if necessary and identify by block number)					
<p>The soliton approach of describing the operation of a microwave crossed-field amplifier (CFA) is experimentally investigated using the Varian SFD-262 S-Band CFA as the test vehicle. Theoretical predictions of voltage characteristics with corresponding observed data show close agreement over a wide range of magnetic field values. A detailed description of the experimental process is given as well as a working introduction to soliton theory.</p>					
20 DISTRIBUTION / AVAILABILITY OF ABSTRACT <input type="checkbox"/> UNCLASSIFIED / UNLIMITED <input checked="" type="checkbox"/> SAME AS REPORT <input type="checkbox"/> DUE TO USERS			21 ABSTRACT SECURITY CLASSIFICATION UNCLASSIFIED		
22a NAME OF RESPONSIBLE INDIVIDUAL Andrew E. Chrostowski, 1Lt, USAF			22b TELEPHONE (Include Area Code) (315) 330-4381		22c OFFICE SYMBOL RADC (OCTP)

DD FORM 1473, 84 MAR

81 APR edition may be used until exhausted.  
All other editions are obsolete.

SECURITY CLASSIFICATION OF THIS PAGE

UNCLASSIFIED

# ABSTRACT

The soliton approach of describing the operation of a microwave crossed-field amplifier (CFA) is experimentally investigated using the Varian SFD-262 S-band CFA as the test vehicle. Theoretical predictions of voltage characteristics with corresponding observed data show close agreement over a wide range of magnetic field values. A detailed description of the experimental process is given as well as a working introduction to soliton theory.

Accession For	
NTIS CRA&I	<input checked="checked" type="checkbox"/>
DTIC TAB	<input type="checkbox"/>
Unannounced	<input type="checkbox"/>
Justification	
By	
Distribution /	
Availability Codes	
Dit	Avail and/or Special
A-1	



## ACKNOWLEDGMENTS

In pursuing this investigation, I have become deeply indebted to a number of individuals for making contributions at various points. Among these, special consideration must be given to the AFTER program at the University of Utah and Dr. Richard W. Grow whose respective support and supervision made this research possible. Additionally, the Varian Beverly Microwave Division must be thanked for providing the technical expertise and facilities for all experimental work that was performed. I am also most grateful to Gary E. Thomas for supplying the impetus for this investigation and the rest of the tube engineering personnel at Varian for critical appraisals and enlightening discussions of the subject matter.

# TABLE OF CONTENTS

	<u>Page</u>
ABSTRACT . . . . .	ii
ACKNOWLEDGMENTS . . . . .	iii
LIST OF ILLUSTRATIONS AND TABLES . . . . .	vi
I. INTRODUCTION . . . . .	1
II. THE SOLITON CONCEPT; DEFINITIONS AND CHARACTERISTICS . . .	5
III. SOLITON THEORY AS APPLIED TO THE CFA . . . . .	9
IV. VOLTAGE REGIMES OF THE CFA PREDICTED BY SOLITON THEORY . . .	16
1. True Synchronous Voltage ( $V_{se}$ ) . . . . .	16
2. Soliton Voltage ( $V_s$ ) . . . . .	17
3. Maximum Operating Voltage ( $V_{max}$ ) . . . . .	18
4. Phase Transition Voltage ( $V_{pt}$ ) . . . . .	19
V. PURPOSE AND EXPERIMENT VEHICLE . . . . .	20
1. Purpose of Experiments . . . . .	20
2. The CFA: Generic Designations . . . . .	20
3. The Varian SFD-262 CFA . . . . .	24
VI. MAGNETIC CIRCUIT . . . . .	26
1. Design Revisions . . . . .	26
2. Calibration of Magnetic Circuit . . . . .	28
VII. EXPERIMENTAL HARDWARE . . . . .	32
1. Operational Setup . . . . .	32
2. Diagnostic Capabilities . . . . .	33
VIII. MEASUREMENT PROCESS . . . . .	38



IX.	GENERATION OF RESULTS . . . . .	41
	1. Experimental Results . . . . .	41
	2. Theoretical Results . . . . .	48
X.	DISCUSSION AND COMPARISON OF RESULTS . . . . .	53
	1. Discussion of Experimental Results . . . . .	53
	2. Discussion of Theoretical Results . . . . .	54
	3. Comparison Between Experimental and Theoretical Results . . . . .	55
XI.	CONCLUSIONS AND FUTURE WORK . . . . .	59
	REFERENCES . . . . .	61

# LIST OF ILLUSTRATIONS AND TABLES

<u>Figure</u>		<u>Page</u>
1	Nonlinearity and dispersion . . . . .	7
2	CFA geometry . . . . .	10
3	Interaction process . . . . .	11
4	Family tree of distributed-emission CFAs . . . . .	22
5	CFA representations . . . . .	23
6	Calibration of magnetic circuit . . . . .	29
7	Magnetic circuit calibration curve . . . . .	31
8	SFD-262 operational chain . . . . .	34
9	Experimental configuration . . . . .	35
10	SFD-262 diagnostics . . . . .	37
11	P-V characteristics . . . . .	42
12	V-I characteristics . . . . .	43
13	Ph-V characteristics . . . . .	44
14	Experimental results . . . . .	49
15	Upturn current versus magnetic field . . . . .	50
16	Maximum power versus magnetic field . . . . .	51
17	Theoretical results . . . . .	52
18	Results comparison . . . . .	56

## Table

1	Experimentally determined regime voltages . . . . .	46
2	Observed upturn current and maximum power values . . . . .	47

## I. INTRODUCTION

The inherent nonlinearities of microwave crossed-field devices have for years plagued the design engineer who, as a result, has had only a few tools to use in the design process. The seeming scarcity of accurate design aids stems from the fact that classical treatments of these high-power microwave tubes such as magnetrons and crossed-field amplifiers (CFAs) have their roots in linear and quasi-linear theory. Such linear treatments of device operation have successfully modeled a number of other tube counterparts such as traveling-wave tubes (TWTs) and klystrons, but have proved thoroughly inadequate for the crossed-field device.

In order to form a backdrop to the substance of this investigation, the previous attempts at and limitations of describing crossed-field devices must be briefly addressed.

Any attempt developed over the past forty years to describe crossed-field device operation has centered on electron beam-RF wave interactions taking place inside the tube. A complete understanding of this interaction process would yield valuable information to the designer and the design process. Previous efforts in describing electron beam-RF wave interactions can be broken down into two areas. These encompass linear and quasi-linear theory and computer modeling.

The classical texts<sup>1-3</sup> have treated the first area rather extensively. From these treatments, one can further subdivide linear theory into beam equilibria arguments and coupled mode relations.

Understanding the equilibria states of electrons in crossed-field

devices has been the subject of extensive effort by investigators.<sup>1,2</sup> One treatment used was Brillouin or laminar flow in which the electrons move in a path parallel to the cathode surface forming a theoretical "hub" around the cathode. Conversely, looping orbits of the electrons have been investigated and have been postulated to be the cause of spokes in the interaction space. As recent research<sup>4</sup> indicates, neither of these simplified models is absolutely correct and a realistic approach would incorporate some combination of these effects. Even so, a beam equilibrium approach gives little insight into crossed-field device operation. This is principally due to the fact that RF circuit electric field strength in these devices is of such intensity that it drastically alters the equilibrium state of the beam. These RF effects are not integral to either of the classical treatments of this subject.

Coupled mode theory<sup>5</sup> utilizes an approach in which there is a coupling mechanism between an electron beam mode and a slow wave circuit mode. Such coupling is weak by nature and can only describe small perturbations made by the beam on the slow wave and vice versa. However, in crossed-field devices, the large beam perturbations present eventually cause the transport of electrons from cathode to anode. This transport indicates a strong coupling mechanism between the beam and circuit wave, thereby invalidating classical coupled mode theory.

The problems associated with linear theory led researchers to then attempt by means of the computer to simulate the environment inside the interaction space of crossed-field devices.<sup>6-8</sup> First attempts were quasi-static in nature in which a single wavelength in a moving frame of reference centered on the wave itself was simulated. Other codes were

similar, but modeled multiple wavelengths in a stationary frame.

State-of-the-art computer codes<sup>4,9,10</sup> feature time-stepped particle-in-cell (PIC), fully relativistic 2-1/2 dimension solutions to Maxwell's equations in the interaction space. Although the results of these codes are promising, the computer time required to model a sufficient number of particles (usually a few thousand) to assure a complete picture of device operation is in many cases prohibitive. As an example, it takes 10 CPU hours of computer time on a DEC VAX 11/780 to simulate just 1 ns of operation of an 18 GHz magnetron. A minimum of 10 ns is required to draw a somewhat complete picture of device operation.<sup>11</sup> At this time, there is still a trade off between the fineness of detail and the amount of computer time needed to produce a particular simulation. As a result, coarse simulations yield only limited amounts of information and thus are not valuable as a design tool.

Until recently, both of the above methods were the only satisfactory methods (although inaccurate and/or costly) available to the tube industry as a whole.

With the upsurge in interest in electron devices in the last few years (gyrotrons, relativistic magnetrons, etc.), it was clear that new methods were required to model device operation. A new approach to analytically model the nonlinear interaction between electrons and the slow wave circuit in a microwave crossed-field amplifier was developed. This new approach is based on the soliton concept.<sup>12</sup>

This investigation is divided into two parts. A working introduction to soliton theory is given in the first part. This introduction is done on both a pure and applied level in order to provide the necessary

background to this subject and relate it to concepts that are familiar to the microwave tube community. The second part of this effort discusses experimental work done on a specific microwave CFA. This work was done to verify predictions made by soliton theory.

## II. THE SOLITON CONCEPT: DEFINITIONS AND CHARACTERISTICS

The soliton concept is one that has manifested itself in nature a number of times in the past, but has only recently been the subject of formal investigation.<sup>13-16</sup> This chapter introduces the soliton in terms of definitions and characteristics in order to solidify these conceptions.

First reported by John Scott-Russell in 1844,<sup>17</sup> he noted that water waves in a channel had unique properties after some initial excitation from a boat. The properties he had viewed were that of a wave shape that was a rounded, smooth, and well defined heap of water that propagated some distance without change of shape or speed even after collision with water waves of similar type.

In 1895, Korteweg and deVries provided an analytic basis for Scott-Russell's observation by developing an equation for the motion of shallow water waves.<sup>18</sup> This was to become known as the KdV equation. The relation for this motion was a partial differential equation that had a solution of the form of  $\text{sech } x$ . In time, other partial differential equations were found to have the same type of solutions. Besides the KdV equation, other examples of this form of equation are the nonlinear Schrodinger and sine-Gordon equations. These and others are cataloged in the references.<sup>13</sup> With the advent of the modern computer, investigators were given a freer hand in defining the waves produced from these solutions, later to be identified as solitary waves.

It is now important before proceeding to make the following fundamental definitions for the sake of clarity.

A traveling wave is a solution of a particular wave equation that is any recognizable signal that can be transferred from one part of a medium to another. In addition, it must also have a discernible velocity and period of propagation at any instant of time.

Consider now a particular type of traveling wave such that its period is infinite. Therefore, over a particular interval of interest (a localized interval), only one signal (wave) is present. Thus, this remaining single or "solitary" wave can therefore be recognized as simply a localized traveling wave.

Finally, given the above concepts, a soliton is defined to be a solitary wave solution to a wave equation which preserves its speed and shape upon collision with others like itself, except for a possible phase shift.

Given these definitions, it is now interesting to note what conditions can produce solitons. A soliton can best be understood as being a balance between nonlinearity and dispersion, as shown in Fig. 1. Nonlinearity is the effect which causes a waveform to peak and break, while dispersion is the tendency of frequency components to spread. The presence of one of these effects without the other does not produce solitons, since the aforementioned balance is violated. A shock is the result of an imbalance of these two effects.

An interesting aspect of soliton behavior is that any arbitrary initial excitation of a system that will support solitons will decompose into a series of solitons of different amplitudes and velocities. This effect is directly analogous to a Fourier series representation, except that some other parameter besides frequencies (as in Fourier analysis)



### **DISPERSION**



### **NONLINEARITY**



### **SOLITON (DISPERSION + NONLINEARITY)**



### **SHOCK (DISPERSION - NONLINEARITY)**



Fig. 1. Nonlinearity and dispersion.

governs soliton behavior. As an example that will have further interest here, the soliton governing parameter of the nonlinear Schrodinger equation is the energy levels of a nonlinear potential well. Thus, like a Fourier series, this feature allows any arbitrary excitation to be treated in a true analytic fashion.

With this brief introduction to soliton theory and behavior, it is now time to address the connection between soliton theory and microwave CFAs. As previously mentioned, soliton behavior represents a balance between nonlinearity and dispersion. Since the CFA has historically been recognized to possess both of these qualities, prudent reasoning would conclude that this device is a likely candidate for a soliton analysis of its behavior. The next chapter of this paper treats the CFA from a soliton point of view.

### III. SOLITON THEORY AS APPLIED TO THE CFA

The approach used assumes that CFA operation is based on an electron cloud (electron plasma), RF circuit wave interaction in which the RF wave travels through the electron cloud. This is better shown in terms of the device geometry and interaction process of Figs. 2 and 3. Solitons result from the combination of this circuit wave and the electron cloud which becomes trapped in bunches and forms spoke-like shapes. The CFA soliton is the hyperbolic secant variation in the x-directed RF electric field which spatially occurs at the outer edge of the Brillouin hub.

A nonlinear, partial differential equation having soliton solutions is derived by treating the effect of the electrons on the RF wave and the effect of the RF wave on the electrons separately. These two effects are responsible for the dispersion and nonlinearity, respectively, in the system.

Treating the effect of the electrons on the RF wave first, a nonlinear dispersion relation is derived from the kinetic theory of plasmas by using the Vlasov-Maxwell equation:

$$\frac{\partial f}{\partial t} + \vec{v} \cdot \nabla_r f - e(\vec{E} + \vec{v} \times \vec{B}) \cdot \nabla_v f = 0 \quad (1)$$

where  $f$  is some electron distribution function,  $v$  is electron velocity,  $E$  and  $B$  are the electric and magnetic fields, and  $e$  is electronic charge. Using perturbation techniques with the method of characteristics as in Krall and Trivelpiece<sup>19</sup> and retaining the dominant RF

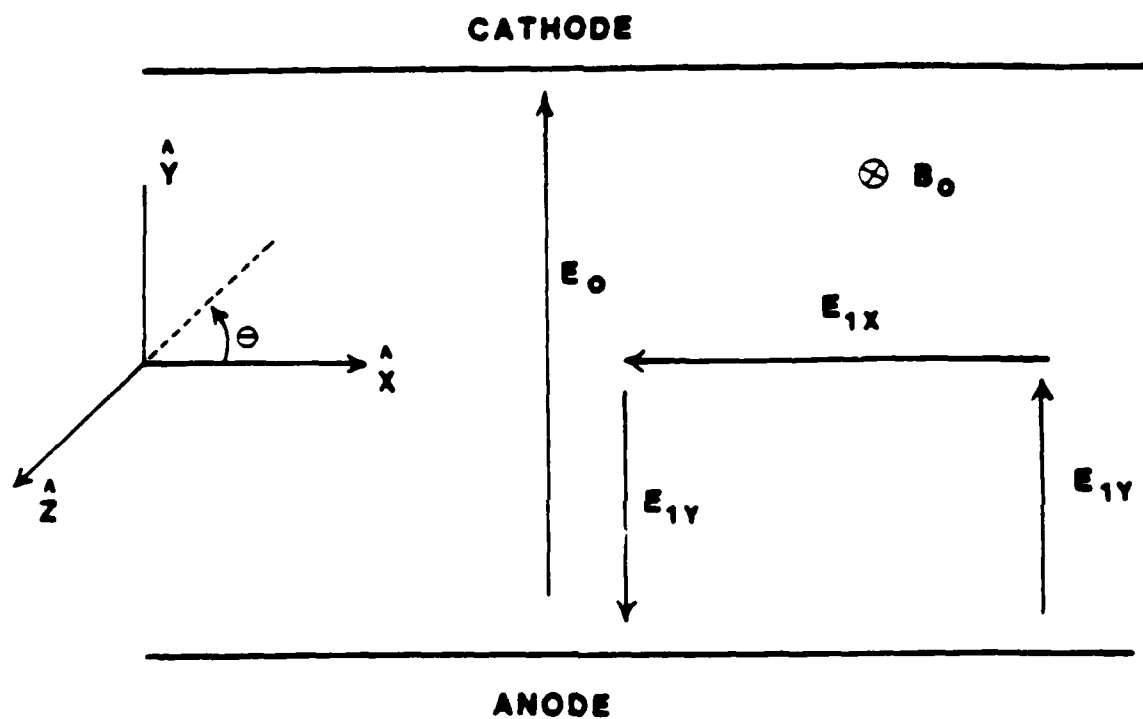


Fig. 2. CFA geometry.

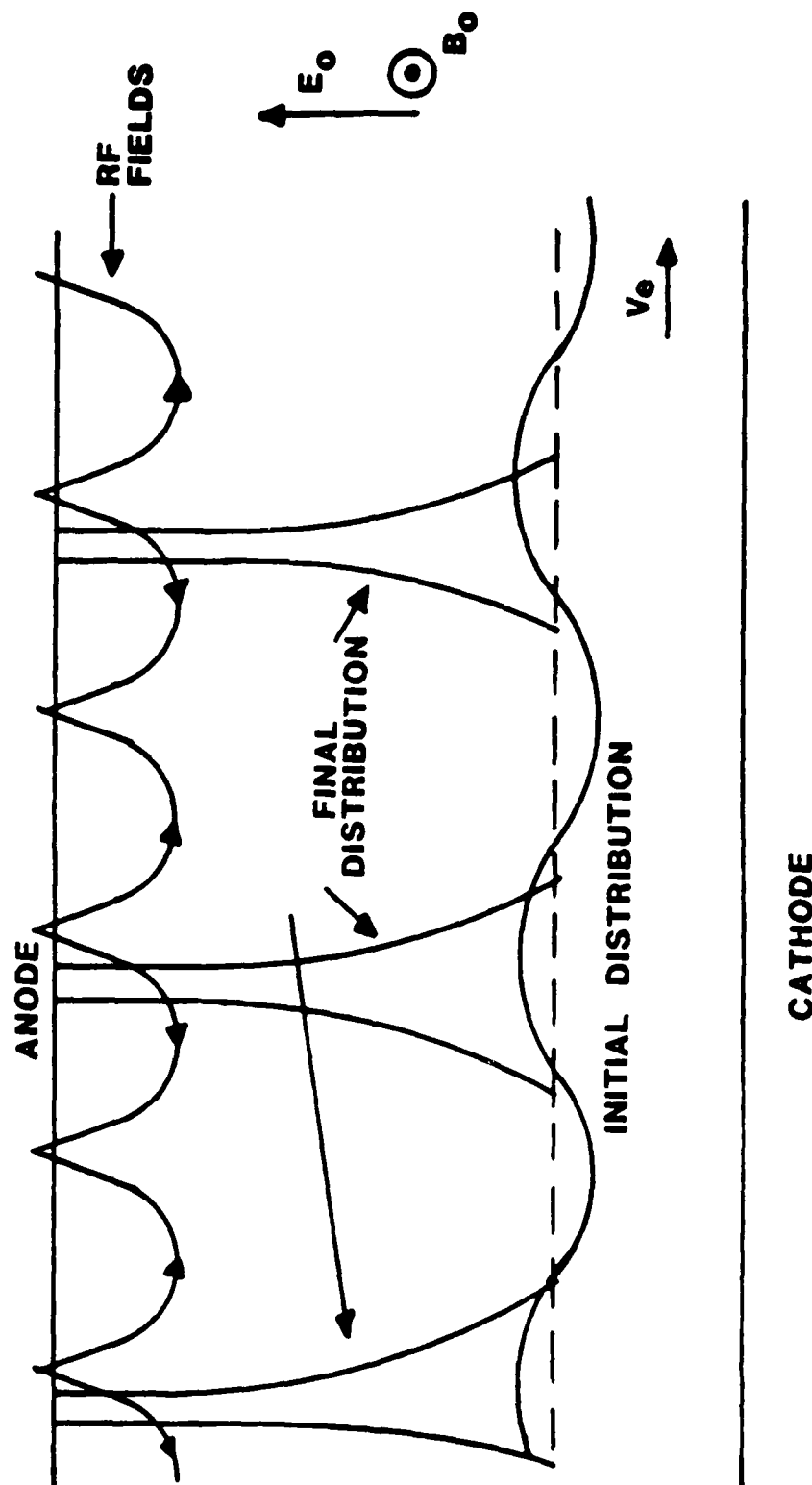


Fig. 3. Interaction process.

electric field component (x-directed) yields the following equation:

$$A_0 \frac{\partial^2 E_x}{\partial x^2} + B_0 \frac{\partial^4 E_x}{\partial x^4} + C_0 \frac{\partial^2 E_x}{\partial z^2} + D_0 \frac{\partial^2 E_x}{\partial t^2} = 0 \quad (2)$$

The details of this derivation are beyond the purpose of this paper, but are contained in the references.<sup>20</sup>

The second effect, that of the RF wave on the electrons, is given by the ponderomotive force.<sup>21</sup> This force is nonlinear in nature and is the result of time and spatial variations in the electric and magnetic fields. An expression describing the ponderomotive force is given by

$$f_{NL} = - \frac{1}{4} \frac{e^2}{m\omega^2} \nabla E^2 \quad (3)$$

where

$$E^{(1)} = E^{(1)}(r_0) \cos \omega t + (\delta r^{(1)} \cos \omega t \cdot \nabla) E^{(1)}(r) \cos \omega t \quad (4)$$

is an oscillating electric field shown expanded by means of a Taylor series. The first term of Eq. 4 will time average to zero, but the second term will not, resulting in a nonlinear force given by Eq. 3. The ponderomotive force will form bunched electrons in those areas where the gradient of the electric field is zero, since the force on the electrons at those points is zero. The electron bunches will lead to the formation of spoke-like shapes as those electrons are then transported to the anode under the influence of  $\vec{E}_{RF} \times \vec{B}_0$  motion.

This bunching can be seen as a slowly varying electron modulation of the dispersion relation of Eq. 2. The perturbed density can be found by using an equation of fluid dynamics<sup>22</sup> that is proportional to the oscillating electric field, or

$$n_1 = |E_1|^2 \quad (5)$$

where  $n_1$  is the perturbed density.

The total density  $n$  is given by the sum of the zero-order density ( $n_0$ ) and perturbed density, or

$$n = n_0 + n_1 \quad (6)$$

Substituting Eq. 6 into Eq. 2 results in a nonlinear equation for the dominant (x-directed) electric field component. This equation describes the wave behavior as it travels through the nonlinear electron cloud and is given by

$$A_0 \frac{\partial^2 E}{\partial X'^2} + B_0 \frac{\partial^4 E}{\partial X'^4} + C_0 \frac{\partial^2 E}{\partial Z'^2} + F_0 \frac{\partial^2 E}{\partial Y'^2} + D_0 \frac{\partial^2 E}{\partial t'^2} + J_1 |E|^2 E = 0 \quad (7)$$

The coefficients of Eq. 7 are rather lengthy, depend on tube parameters, and are omitted here for simplicity.

The solution of Eq. 7 is not readily attainable, but can be reduced to a solvable form by using a method known as the multiple time scales perturbation technique.<sup>23</sup> This technique orders the importance of the derivatives of Eq. 7 according to how rapidly they vary with

time. From this perturbation method, a second order equation of the form

$$-2i\omega D_o \frac{\partial E}{\partial t} - 2B_o K_x^2 \frac{\partial^2 E}{\partial X'^2} + C_o \frac{\partial^2 E}{\partial Z'^2} + F_o \frac{\partial^2 E}{\partial Y'^2} + J_1 |E|^2 E = 0 \quad (8)$$

results. Using a change of variables, Eq. 8 can be written as

$$i \frac{\partial E}{\partial t} \pm \frac{\partial^2 E}{\partial X^2} \pm \frac{\partial^2 E}{\partial Z^2} \pm \frac{\partial^2 E}{\partial Y^2} + |E|^2 E = 0 \quad (9)$$

with the coefficients again omitted for simplicity. Comparing this result with the nonlinear Schrodinger equation,

$$i \frac{\partial E}{\partial t} + \frac{\partial^2 E}{\partial X^2} + |E|^2 E = 0 \quad (10)$$

shows that Eqs. 9 and 10 are identical, except for the addition of two differential terms. The importance of this comparison is the fact that the nonlinear Schrodinger equation is known to have soliton solutions. The effect of the additional terms has been shown by conservation of energy arguments<sup>20</sup> and stability analysis<sup>24</sup> to result in wave growth or decay, depending on the signs of the coefficients in Eq. 9. Thus, Eq. 9 can have soliton solutions that either grow or decay.

Listing the various forms of Eq. 9 while keeping the above statements in mind yields

$$i \frac{\partial E}{\partial t} + \frac{\partial^2 E}{\partial X^2} - \frac{\partial^2 E}{\partial Z^2} - \frac{\partial^2 E}{\partial Y^2} + |E|^2 E = 0 \quad (\text{growing solitons}) \quad (11)$$



$$i \frac{\partial E}{\partial t} + \frac{\partial^2 E}{\partial X^2} + \frac{\partial^2 E}{\partial Z^2} + \frac{\partial^2 E}{\partial Y^2} + |E|^2 E = 0 \quad (\text{decaying solitons}) \quad (12)$$

$$i \frac{\partial E}{\partial t} - \frac{\partial^2 E}{\partial X^2} - \frac{\partial^2 E}{\partial Z^2} - \frac{\partial^2 E}{\partial Y^2} + |E|^2 E = 0 \quad (\text{growing shocks}) \quad (13)$$

$$i \frac{\partial E}{\partial t} - \frac{\partial^2 E}{\partial X^2} + \frac{\partial^2 E}{\partial Z^2} + \frac{\partial^2 E}{\partial Y^2} + |E|^2 E = 0 \quad (\text{decaying shocks}) \quad (14)$$

In terms of this investigation, Eqs. 11 and 12 are of interest. As just mentioned, the signs of the coefficients determine either the growth or decay of solitons and thus are used to predict amplification regimes in the CFA. Since the coefficients are a function of tube parameters, prediction of amplification regimes is readily possible. Said another way, the knowledge of the amplification regimes beforehand can allow the design of tube parameters without the usual pitfalls (excessive time, money, etc.) associated with traditional CFA development. This is the power of the soliton approach. It allows the analytic solution of a nonlinear time dependent system, in this case, the CFA. As a result, it describes device behavior not predictable by other means.

The next chapter of this paper details the CFA amplification regimes predicted by soliton theory. These amplification regimes are described in terms of the voltage characteristics of the CFA.

#### IV. VOLTAGE REGIMES OF THE CFA PREDICTED BY SOLITON THEORY

The changes of the signs of the coefficients associated with Eqs. 11 through 14 represent transitions between different voltage regimes in the CFA. Making use of this concept, it is now time to define these voltage regimes in both a qualitative as well as quantitative manner.

The regimes of interest in this investigation are given by the following designations: the true synchronous voltage ( $V_{se}$ ), soliton voltage ( $V_s$ ), maximum operating voltage ( $V_{max}$ ), and phase transition voltage ( $V_{pt}$ ). Each of these will be addressed separately in the following discussion.

##### 1. True Synchronous Voltage ( $V_{se}$ )

The true synchronous voltage ( $V_{se}$ ) is the voltage where the electron and the circuit wave phase velocity are equal. The term "true" is included in the above description, since  $V_{se}$  takes into account cathode-to-anode directed RF electric fields. It is also associated with the beginning of the presence of solitons in the interaction area. The classical theory counterpart of the synchronous condition has been the Hartree voltage ( $V_H$ ).<sup>2</sup> However, the condition associated with the Hartree voltage deals only with dc effects, thereby invalidating it as a true synchronous voltage. The Hartree voltage is given by

$$V_H = \frac{1}{2} B_0 \omega (r_a^2 - r_c^2) - \frac{\omega^2 r_a^2}{2\eta} \quad (15)$$

where

$r_a$  = anode radius

$r_c$  = cathode radius

$B_0$  = operating magnetic field

$\eta$  = electronic charge to mass ratio

$\omega$  = operating frequency

$V_{se}$  is determined by approximating the transition from operating in the theoretical Brillouin hub condition to operating with a uniform electron density in the interaction area. Approximate methods for determining this voltage have been made in the past with good results.<sup>\*25</sup> Recent work<sup>26</sup> has produced an exact expression for  $V_{se}$  in terms of  $V_H$  to be

$$V_{se} = V_H \left[ 1 + \frac{\omega_c}{\omega} \left( \frac{\epsilon}{1 - \epsilon} \right) \right] \quad (16)$$

where

$\omega_c$  = cyclotron frequency

$\epsilon$  = ratio of the y-directed RF electric field to the dc electric field (see Fig. 2).

The form of Eq. 16 shows that it reduces to the Hartree voltage if the cathode-anode RF electric field is considered zero ( $\epsilon = 0$ ).

## 2. Soliton Voltage ( $V_s$ )

As the operating voltage of the CFA is raised above  $V_{se}$ , the existence of solitons becomes more abundant in the interaction area.

---

\*  $V_{se}$  is designated as  $V_{sync}$  in this reference.

The soliton voltage ( $V_s$ ) is the point where solitons completely fill the interaction area. To determine this point, the electron density is assumed to be uniform throughout the interaction area. It has been shown<sup>25</sup> that the soliton voltage can be obtained from the coefficients of the nonlinear Schrodinger equation,

$$V_s = \omega d B_o / k_l \quad (17)$$

where

$d$  = cathode-anode spacing

$k_l$  = circuit wave number

and the other parameters are as defined before.

The derivation yielding Eq. 17 assumes that there is a minimum electron density for the soliton solution to exist. At this time, this value is thought to be approximately  $1 \times 10^{11}$  electrons/cm<sup>3</sup>.

### 3. Maximum Operating Voltage ( $V_{max}$ )

Above the soliton voltage, solitons no longer fill the interaction area. Rather, shocks appear starting at the cathode and filling the interaction area as the operating voltage is increased. The voltage where solitons no longer exist in the interaction area is designated as the maximum operating voltage ( $V_{max}$ ). This voltage is also the value where operation ceases at the desired frequency. The scheme for determining  $V_{max}$  is rather complicated and involves an iterative process. This process is used to obtain the theoretical curve for  $V_{max}$  presented later.

#### 4. Phase Transition Voltage ( $V_{pt}$ )

$V_{se}$  not only describes the true synchronous velocity in the interaction area of the CFA, but also indicates where a change in the slope of the phase shift of the device should occur. The details of this argument appear in the literature.<sup>25</sup> The phase transition voltage ( $V_{pt}$ ) is thus another means to verify the values obtained for  $V_{se}$ . It is used in that capacity in the data reduction process.

## V. PURPOSE AND EXPERIMENT VEHICLE

### 1. Purpose of Experiments

The purpose of the experiments described here is the verification of a soliton analysis of a crossed-field amplifier at the S-band of microwave frequencies. Previous experiments regarding verification of soliton theory using the CFA have been limited both in scope and to C-band frequencies.<sup>12,20,25</sup> The intent of this effort is to broaden the previous work in both these areas. This is done by providing a much larger data base and by using a completely new experimental vehicle at a different frequency band.

### 2. The CFA: Generic Designations

Before discussing the operating parameters of the specific crossed-field amplifier used in this investigation, it is worthwhile to consider the characteristics associated with the generic CFA classification.

The birth of the crossed-field amplifier was an outgrowth of the successful development of the magnetron oscillator which was the topic of much research during World War II. Development of the CFA, however, did not begin in earnest until the early to mid-1950s. The intent of this effort was to develop a high-efficiency microwave amplifier based on the same type of interaction principles found in the magnetron.

The crossed-field amplifier can be classified into a number of categories based on various properties.

One of the most fundamental of these classifications is the emission process. There are basically two types that have been used to date. They are referred to as the injected-beam and distributed-emission versions.

The injected beam format of the CFA is not unlike that found in the O-type TWT. A beam current is produced from an electron gun and directed into a RF wave supported on a slow wave structure. Due to insufficient performance capabilities (low S/N ratio, tendency toward band edge oscillations), this type of CFA has never gained wide acceptance by the end user community.

The second type of CFA is based heavily on the operating concepts found in the magnetron. In this case, the cathode provides current throughout the intersection area and is called a distributed-emission device. As in the magnetron, device operation is heavily dependent on secondary emission, although in the CFA an unheated or "cold" cathode is employed. The combination of electric fields associated with the applied cathode-to-anode voltage and the RF driving signal is enough to start and sustain the emission process.

Differences in distributed-emission CFAs can include the geometrical format employed and type of microwave circuit utilized. These differences are summarized in the family tree shown in Fig. 4. In addition, two CFA representations are given in Fig. 5.

In terms of performance, the CFA has a number of noteworthy properties.<sup>27</sup> They have found application in frequencies ranging from UHF to Ku bands. Instantaneous bandwidths can range from a few to 25 percent for pulse versions and more than an octave for CW devices. This

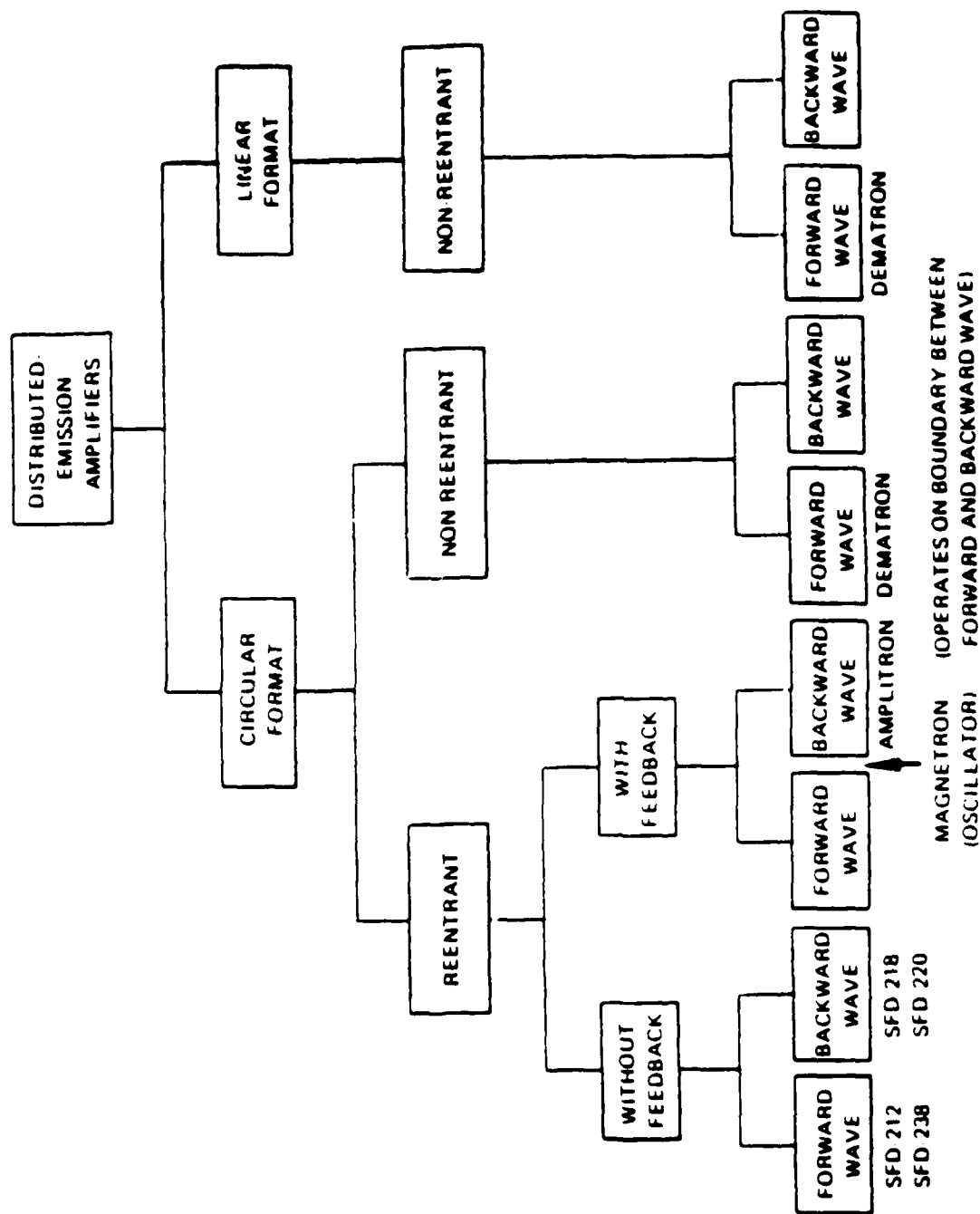
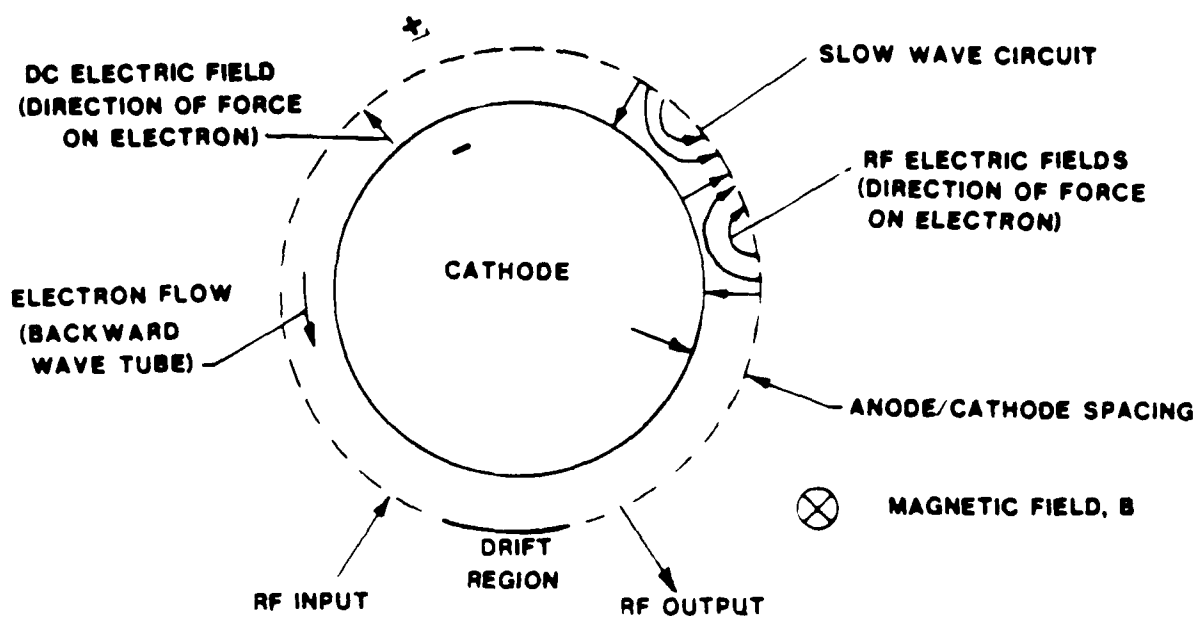
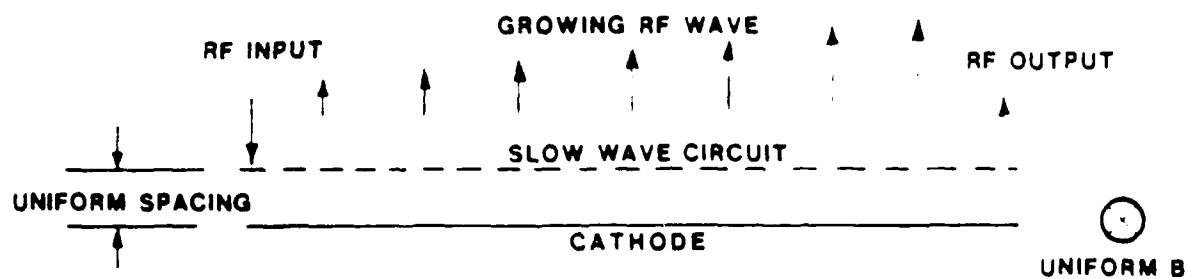


Fig. 4. Family tree of distributed-emission CFAs.





CIRCULAR FORMAT CFA REPRESENTATION



LINEAR FORMAT EQUIVALENT FOR THE CFA

Fig. 5. CFA representations.

latter capability is available in the form of broad bandwidth noise generators. Peak powers of up to several megawatts have been obtained and efficiencies of typically 40 to 65 percent are attainable. Gain of such devices is modest, frequently about 10-13 dB. The above set of characteristics is available using reasonable operating voltages, usually between 15 and 45 kV.

The CFA is used where high-power coupled with high-efficiency operation is a must. Applications include airborne and shipboard radar chains. Because of its characteristics (high efficiency, high power, low gain), it is a perfect match for a klystron or TWT drive source.

### 3. The Varian SFD-262 CFA

The experimental vehicle is the Varian SFD-262 S-band CFA. This device is the double-duty cycle version of another Varian CFA used in the AEGIS combat systems AN/SPY-1B/D phased array radar transmitters. This system is used by the US Navy.

Under operating conditions, the SFD-262 produces a minimum of 125 kW of pulsed RF power from a 6 kW driving signal for a device gain of 13.2 dB. The duty cycle is 1.6 percent, with a corresponding average power output of 2 kW. The nominal operating voltage and current are 12.9 kV and 22 A, respectively. The dc to RF conversion efficiency for the above device is a minimum of 40 percent.

The SFD-262 design has a circular format and employs a forward-wave interaction with a reentrant electron stream. A drift space physically separates the RF input and output ports of the tube. This is done to inhibit electronic feedback. The anode/slow-wave structure is a

double-helix coupled vane circuit and the circular "cold" cathode is initially located on center (in a cylindrical diode configuration), but can be moved off center to improve tube performance. Both the anode and the cathode are water cooled.

The SFD-262 was chosen as the experimental vehicle for a number of reasons.

First, a preliminary data base had been established (although far from complete) in its low magnetic regime of operation. In this case, this regime is defined to be  $\omega_c/\omega < 2.4$ . It was thought that this preliminary data base would aid in the detection of anomalies associated with new data taken.

Second, the SFD-262 was in its preproduction phase providing different design iterations for experimental use. At least three different versions of this CFA were available for test purposes. This feature made comparisons between versions possible, allowing a more complete picture of CFA operation.

Finally, this tube had a computer controlled data acquisition system already in place, allowing timely collection of extensive amounts of data. This system systemized the often tedious process of data taking and removed human error from the measurement process. This system is detailed in a later chapter of this report.

## VI. MAGNETIC CIRCUIT

### 1. Design Revisions

One of the primary goals of this experimental program was to characterize CFA operation as a function of magnetic field. To provide the greatest flexibility in changing the magnetic field in the interaction area of the SFD-262, the tube was operated in conjunction with an electromagnet. In order to obtain data at high magnetic field values, the electromagnet and associated magnetic circuit had to supply a saturated magnetic field value of at least  $\omega_c/\omega = 3.2$ . However, the existing magnetic circuit could only supply a saturated magnetic field in the tube's interaction area of  $\omega_c/\omega = 2.5$ . This fact necessitated the redesign of the existing magnetic circuit.

Upon inspection of the existing magnetic circuit, the following deficiencies were discovered. The vertical risers of the magnetic circuit were positioned too close to each other, providing a path for excessive leakage flux. In addition, the structure of the magnetic circuit was such that there were more right angles than necessary. These angles could give rise to small localized leakage paths within the circuit itself. Finally, an air gap was discovered between the end of the horizontal portion of the magnetic circuit and the pole pieces of the SFD-262. This anomaly effectively increased the total air gap that had to be driven by the magnetic circuit.

Having identified these deficiencies, it now became the task to correct them and increase the maximum magnetic field.

A first attempt at a new magnetic circuit proved unsuccessful. This circuit design was based on the scheme of providing a low leakage path between the vertical portions, while at the same time providing a maximum flux density at the pole pieces of the SFD-262. To further enhance the available field, the magnetic circuit material was made from G-400 iron, a 95 percent pure iron alloy. The test of this circuit (to be detailed in the next section) produced a saturated field value of  $\omega_c/\omega = 2.5$ , no improvement over the previous design. In reflection, it was seen that too many sharply changing angles were still present in this circuit. Also, not enough metallic contact was present between the vertical and horizontal portions of the circuit, allowing a magnetic flux bottleneck to develop.

A second attempt utilizing the lessons learned from the first attempt was successful. Using the magnetic circuit design from another CFA type as a reference, a second magnetic circuit was designed that corrected the above deficiencies. The magnetic circuit featured tapered angular transitions, a maximum separation between vertical circuit supports and, in general, a more pronounced volume of metal. The latter eliminated any flux bottlenecks. The magnetic circuit also featured slots for positioning the cathode off center while the tube was operating and proper access to the cathode coolant connections. A saturated magnetic field of  $\omega_c/\omega = 3.9$  is available from this configuration. This saturated field value was more than sufficient to conduct the desired experiments.

## 2. Calibration of Magnetic Circuit

In order to know precisely the magnetic field in the interaction area of the SFD-262 during experimentation, calibration of the magnetic circuit was needed. The calibration process resulted in a relationship between the magnetic field available in the interaction region of the CFA and the current in the coils of the electromagnet.

For calibration, a teflon spacer was used to simulate the interaction space of the CFA. Teflon was used, since it is a nonmagnetic material and, therefore, does not perturb the magnetic field profile in the interaction area. Also, it is easily machinable. This spacer had a total of 5 probe points to allow magnetic field characterization of a number of positions within the interaction space.

With the design of the spacer completed, the calibration process began. The calibration setup is shown in Fig. 6.

The magnetic field was measured with a rotating coil gaussmeter. The diagnostics consisted of Rawson-Lush type 723 probe and type 501 indicator. After setting an arbitrary electromagnet coil current, the probe was inserted into the middle probe point (the plane of the interaction space) and moved in and out of the spacer by means of a sliding track until the position corresponding to the interaction space was found. This position corresponded to the point where a maximum field deflection was achieved. This was a correct measurement point, since that had been a design goal in the original tube development.

With the probe fixed at this point, the current of the coil supply was set in precise intervals of 0.1 A and the resulting magnetic field

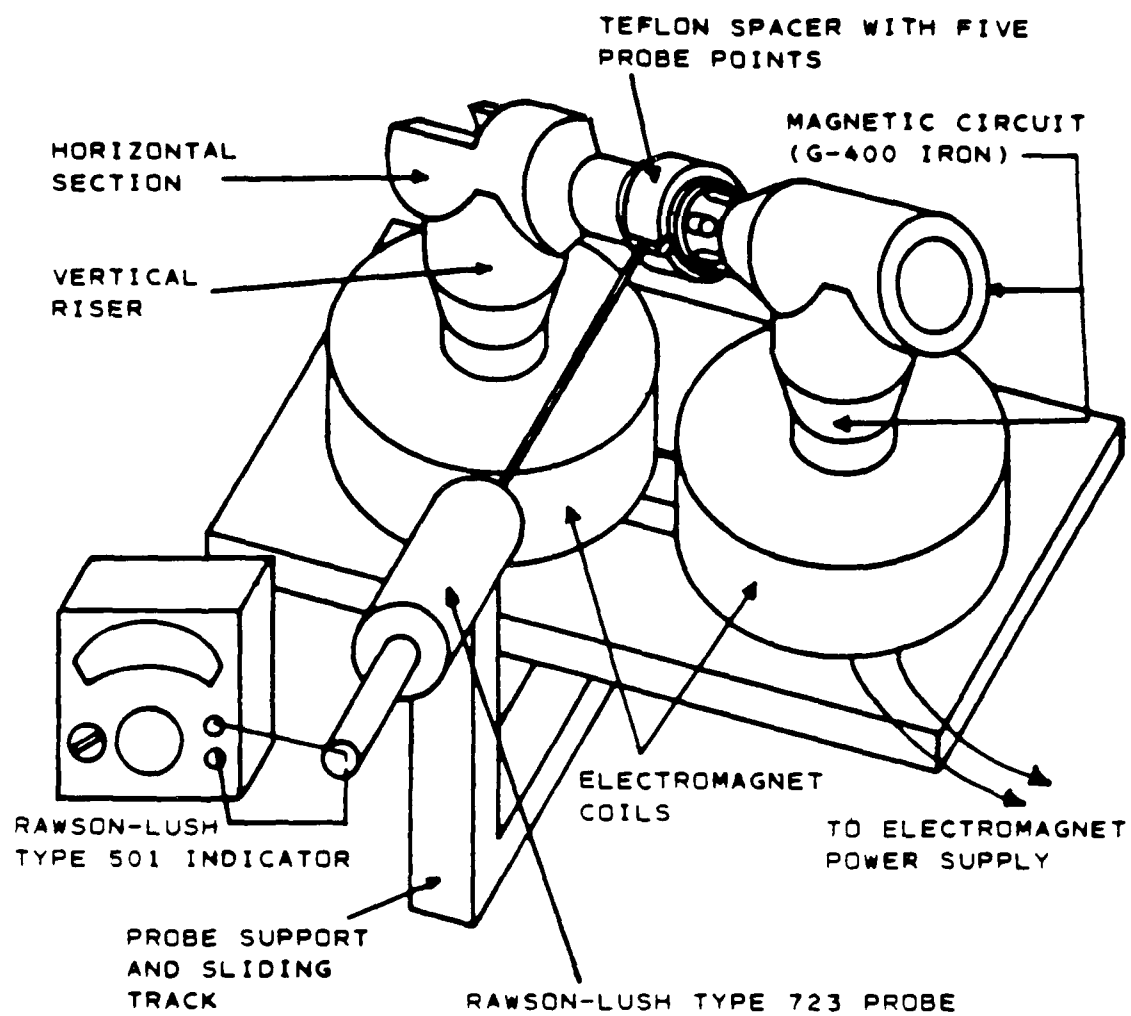


Fig. 6. Calibration of magnetic circuit.

was recorded. This process was done over a range of 0.0 to 4.0 A (the current limit of the electromagnet coil power supply) using first positive and then negative current increments. The result was the familiar hysteresis loop with magnetic field in units of gauss (later converted to  $\omega_c/\omega$  units) recorded as a function of applied electromagnet coil current in units of amperes. This process was repeated several times to prove the validity of the results. The resulting calibration curve is shown in Fig. 7.



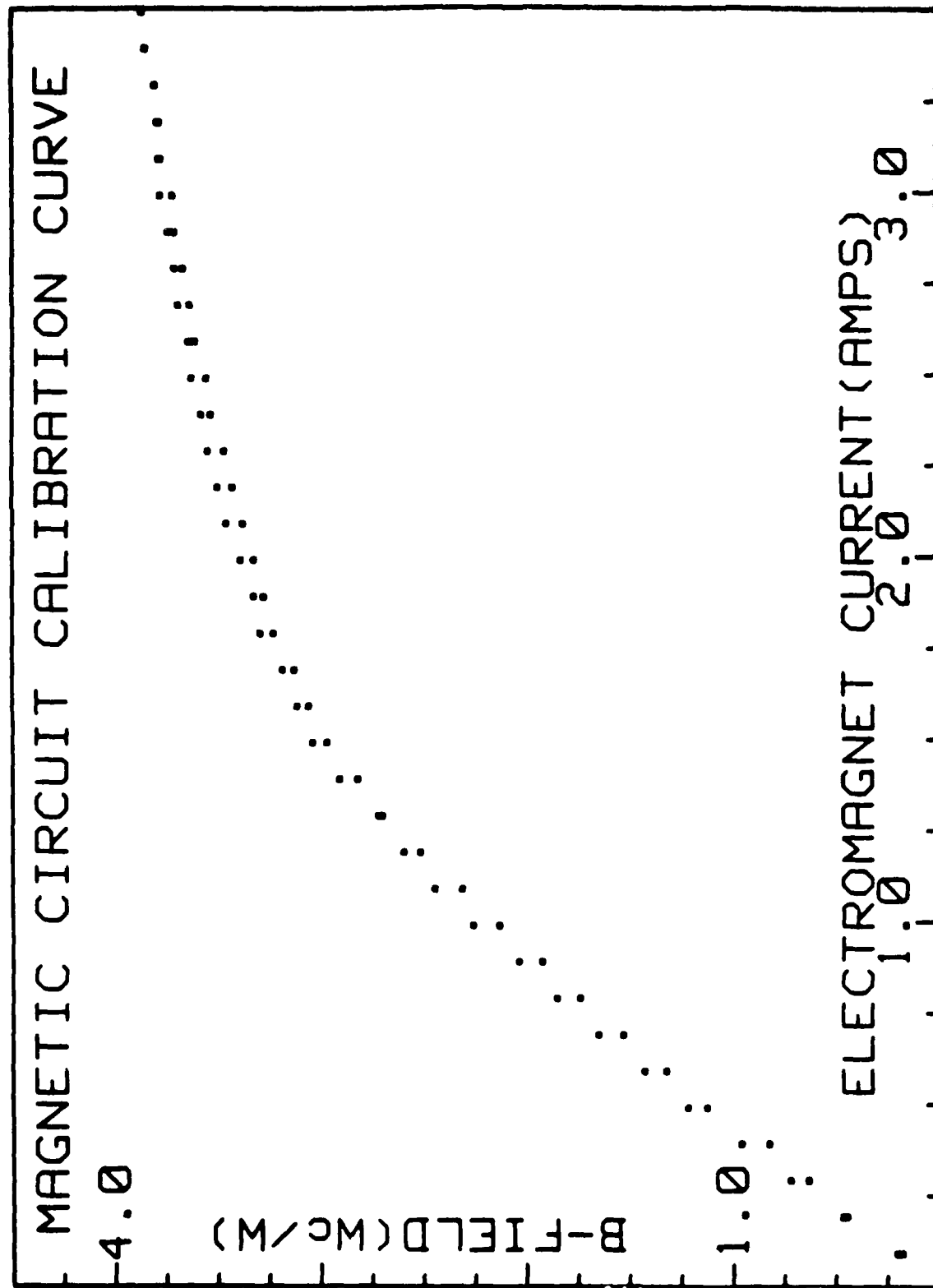


Fig. 7. Magnetic circuit calibration curve.

## VII. EXPERIMENTAL HARDWARE

### 1. Operational Setup

This chapter details the equipment necessary for proper operation of the SFD-262 CFA. This equipment was already in place prior to the experimental process. Interaction with and a general mastering of the operation of this equipment was accomplished and was essential to assure successful experiments.

Generation of the proper RF drive power to the CFA was accomplished using a number of components. The S-band microwave source of power was a Hewlett-Packard 8350A sweep oscillator with 83540A 2.0-8.4 GHz RF plug in. This source provided approximately 10 mW of swept RF power that was in turn used to drive an Alto Scientific Company SK-21221 TWTA. This amplifier provided 20 watts of RF power, but was attenuated by cable loss and a Narda attenuator to the 28 dBm power level. This was the case, since the TWTA was situated with the sweep oscillator inside a screen room while the next driver component was some 30 feet away, and thus an initial power margin was required. This attenuated power level was used to drive a Litton L-5769-59 TWT which produced an 8 kW pulsed RF output. Circulator and inherent waveguide loss reduced this value to a 6 kW minimum which was used to drive the SFD-262 CFA. CFA output power was delivered to a water load.

To produce the required pulsed RF power output, both the SFD-262 CFA and Litton L-5769-59 TWT driver were modulated. In the case of the driver, this was done by pulsing its shadow grid configuration by one modulator while the CFA had its cathode directly pulsed by a second

modulator. The described operational chain is shown in block diagram form in Fig. 8.

The CFA modulator was a floating deck hard tube design featuring constant current operation. It incorporated an Eimac Y-633A tetrode switch tube and could supply the CFA with the maximum values of 20 kV at 30 A if required. An array of interlocks protected both the modulator and CFA. Although the maximum ratings of the modulator were above that used for typical CFA operation, they were utilized for experimental purposes. This was important, since it allowed a view of CFA operation out of its normal parameter range.

In addition to the modulator, other tube connections were required for operation. The CFA had a cathode oxygen replenishing reservoir operating at approximately the 5 V level. In addition to the reservoir, a Varian Vac-Ion Model 921-0015 was attached to the CFA to eliminate gas buildup within the tube. The vac-ion voltage was 3,000 V, while proper CFA operation dictated vac-ion currents of less than 50  $\mu$ A. Finally, the CFA anode body and cathode were externally water cooled at the rate of 0.9 gallons per minute. The SFD-262 is shown in its experimental configuration in Fig. 9 with all connections labeled for clarity.

## 2. Diagnostic Capabilities

The diagnostic capabilities associated with the SFD-262 test station allowed automated testing of device performance. This feature was desirable, since it allowed rapid accumulation of data and eliminated human error.

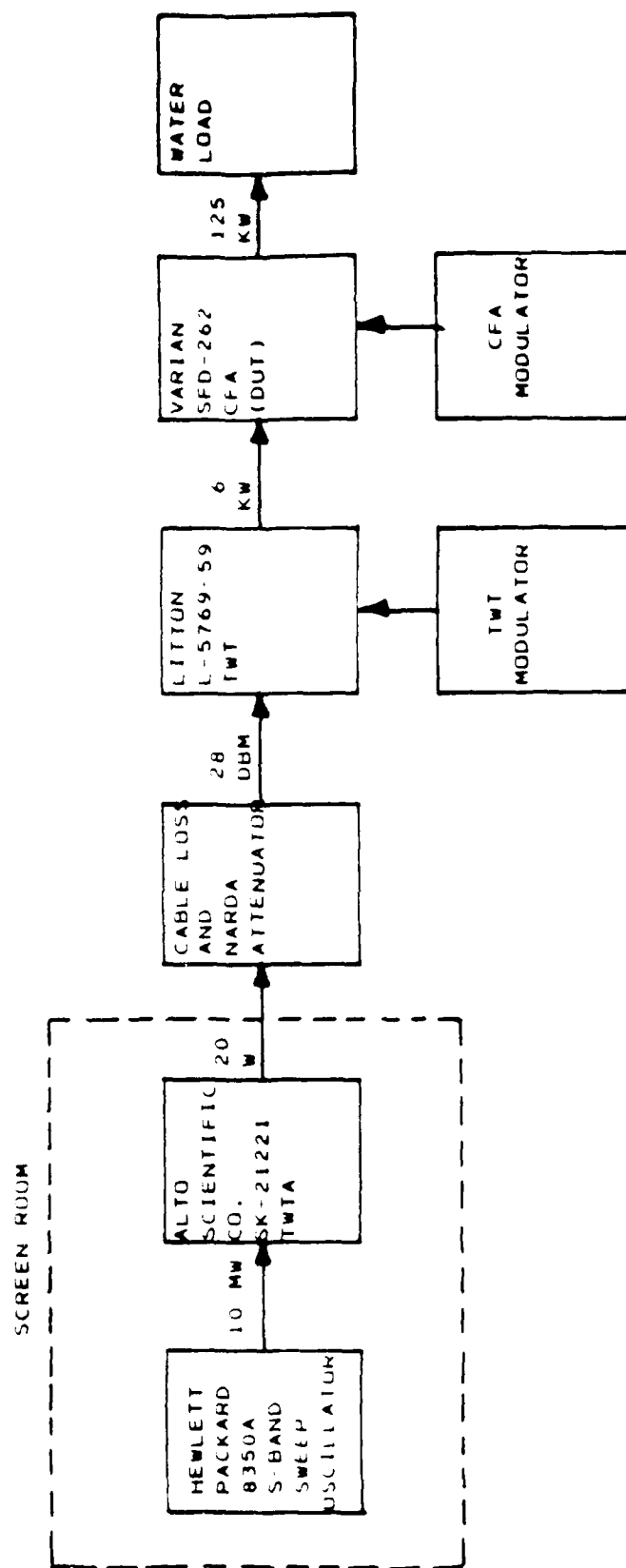


Fig. 8. SFD-262 operational chain.



Fig. 9. Experimental configuration.

In the area of power measurement, a calorimeter attached to the CFA water load was used to establish a RF power reference with other power meters in this system calibrated against this reference. Once this standard was established, coupled power calibrations and measurements were obtained and made by Hewlett-Packard 436A digital power meters for CFA input power, output power, and reflected power.

In a similar fashion, references were established for CFA voltage, current, and phase parameters. All three of these signals were multiplexed to a Fluke 8520A digital multimeter.

The power meters and multimeter described above functioned as analog-to-digital converters allowing computer storage of information provided by these instruments. Once digitized, information was transmitted by means of IEEE-488 information bus to a Hewlett-Packard 85 computer which served as a controller for the entire measurement process. Additional control of the sweep oscillator by the computer allowed measurement of system parameters at a number of frequencies across the operating band. Once the system parameters were recorded, they would be sent to a line printer or plotter additionally controlled by the computer for output purposes. A number of computer programs written specifically for this system were generated to record, process, and present data in various ways. These programs included routines that recorded the major parameters (frequency, voltage, current, output power, phase) and then plotted any one of these parameters versus another. A block diagram showing the extent of the diagnostic capabilities associated with the SFD-262 is shown in Fig. 10.

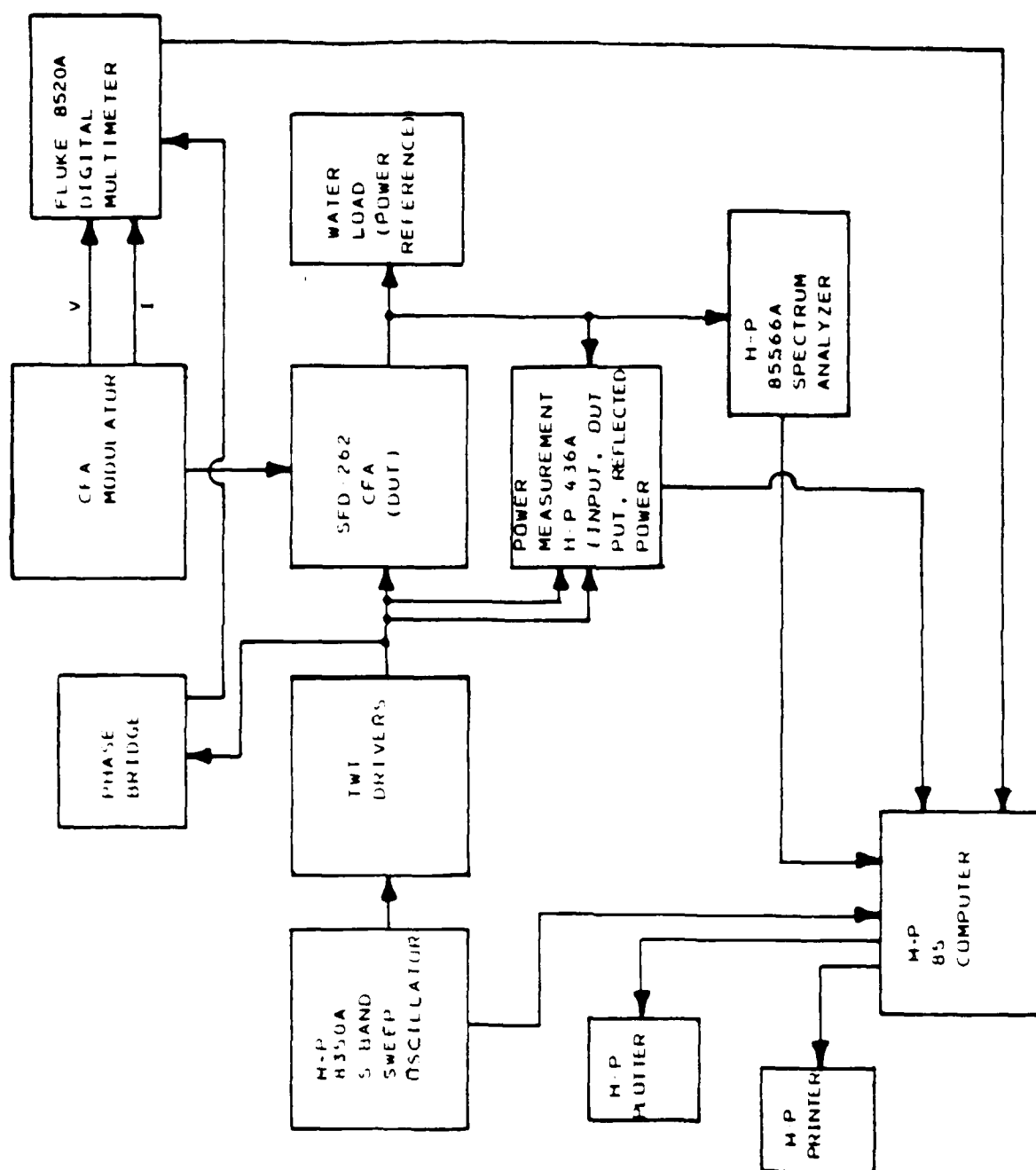


Fig. 10. SFD-262 diagnostics.

## VIII. MEASUREMENT PROCESS

In order to gain the most insight into CFA operation and to make comparisons with soliton theory, the measurement scheme had to be systematic in nature. It was only in this manner that confidence in the results could be high.

All measurements were done at one operating frequency, the CFA's upper band edge. This upper frequency was chosen, since the required operating voltages are lowest because of the forward-wave interaction. Having the lowest possible operating voltages was important because of voltage limitations imposed by the modulator. Thus, this single frequency provided the most useful information. It also limited to an acceptable volume the amount of data collected.

The independent parameters for the experiments are the applied magnetic field and modulator current to the CFA. The magnetic field is an independent variable because it is applied externally to the CFA. Likewise, tube operation is independently determined by the modulator current, since the modulator is a constant current and therefore a current controllable source. This feature is not especially desirable, since the tube can change voltage drastically and its mode of operation rather easily with a small change in current.

Once the independent parameters are set, the dependent parameters are measured. These are the voltage, the RF power output, and relative phase length of the CFA.

A data base was generated by varying both the magnetic field and modulator current over a wide range of values. The magnetic field was



set over the range of  $1.5 < \omega_c/\omega < 3.2$  using 11 different steps. This range of magnetic field corresponded to a regime of low magnetic field to one of high magnetic field and was representative of extremes of device operation. At each of these different magnetic field values, some 15 to 25 data sets consisting of the dependent parameters were recorded after setting the modulator current in convenient intervals. Modulator capabilities set the limits of measurement in this instance. Some 650 data entries were produced from the above process in a hard-copy printout.

There were a number of factors that limited the measurement process.

The foremost of these was the proper operation of the CFA. For a given set of independent parameters (magnetic field, modulator current), the tube would sometimes not function as designed producing out of band oscillations, arcs, and noisy operation. These effects all served to obscure operation at the desired frequency. Data gathering continued until the tube ceased operation at the desired frequency or if it was concluded that further useful information was not possible from the measurement process. These conclusions were based on the ability to record data without noise becoming a masking effect.

In addition to the limits of operation of the CFA, the limits of the modulator posed a problem. As stated in an earlier chapter, the maximum ratings of the modulator (20 kV at 30 A) served to somewhat limit a full performance evaluation of the CFA.

Also, the data acquisition system served to limit the measurement process. Certain required measurements were made by sampling sometimes

noisy parameters (i.e., CFA current) which in turn produced erroneous values for these recorded parameters.

Finally, exact information on the location of the movable cathode within the interaction space was not possible. A theoretical treatment of the CFA assumed a cylindrical diode configuration which was very difficult to achieve in practice. However, the cathode positioning system integral to the SFD-262 design was used to place the cathode "on center" to within the tolerances of that system.

## IX. GENERATION OF RESULTS

### 1. Experimental Results

Having collected the data, the next task was to process it in such a way that a direct comparison between these experimental results and soliton theory could be made. The following discussion outlines the procedure used to transform the "raw" data into finished form ready for comparison.

After establishing the range of the data, a series of three curves were generated at each magnetic field value. These curves consisted of CFA RF power output versus voltage (P-V), voltage versus current (V-I), and relative phase versus voltage (Ph-V). Examples of these curves are shown in Figs. 11, 12, and 13. The entirety of these curves is omitted in order to limit the length of this paper. The curves were generated by means of graphics capabilities of the Hewlett-Packard 9816 personal computer and 7470A plotter.

Having generated the aforementioned curves, each was examined to determine the voltages where characteristic regime changes were present. These voltages showed changes in the operating characteristics of the CFA and would later be compared with predictions made by soliton theory.

The voltages that were noted were, first, an exponential-like to linear transition in RF power output and, second, a roll over or slope decrease in the RF power output. These effects are denoted by the designations  $V_{\text{transition}}$  and  $V_{\text{roll over}}$ , respectively, and examples of these voltages are shown in Fig. 11. Due to the nature of the spacing

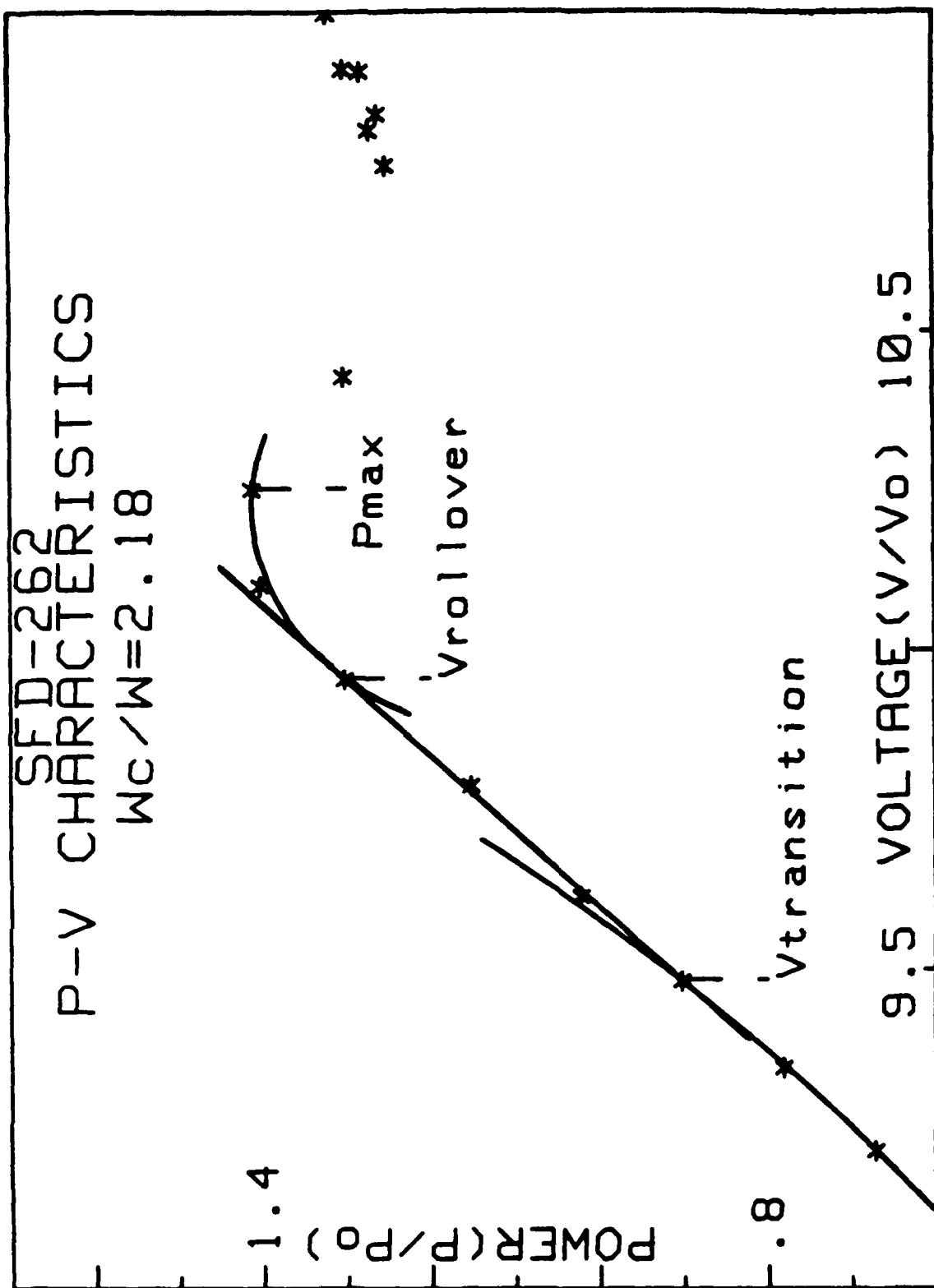


Fig. 11. P-V characteristics.

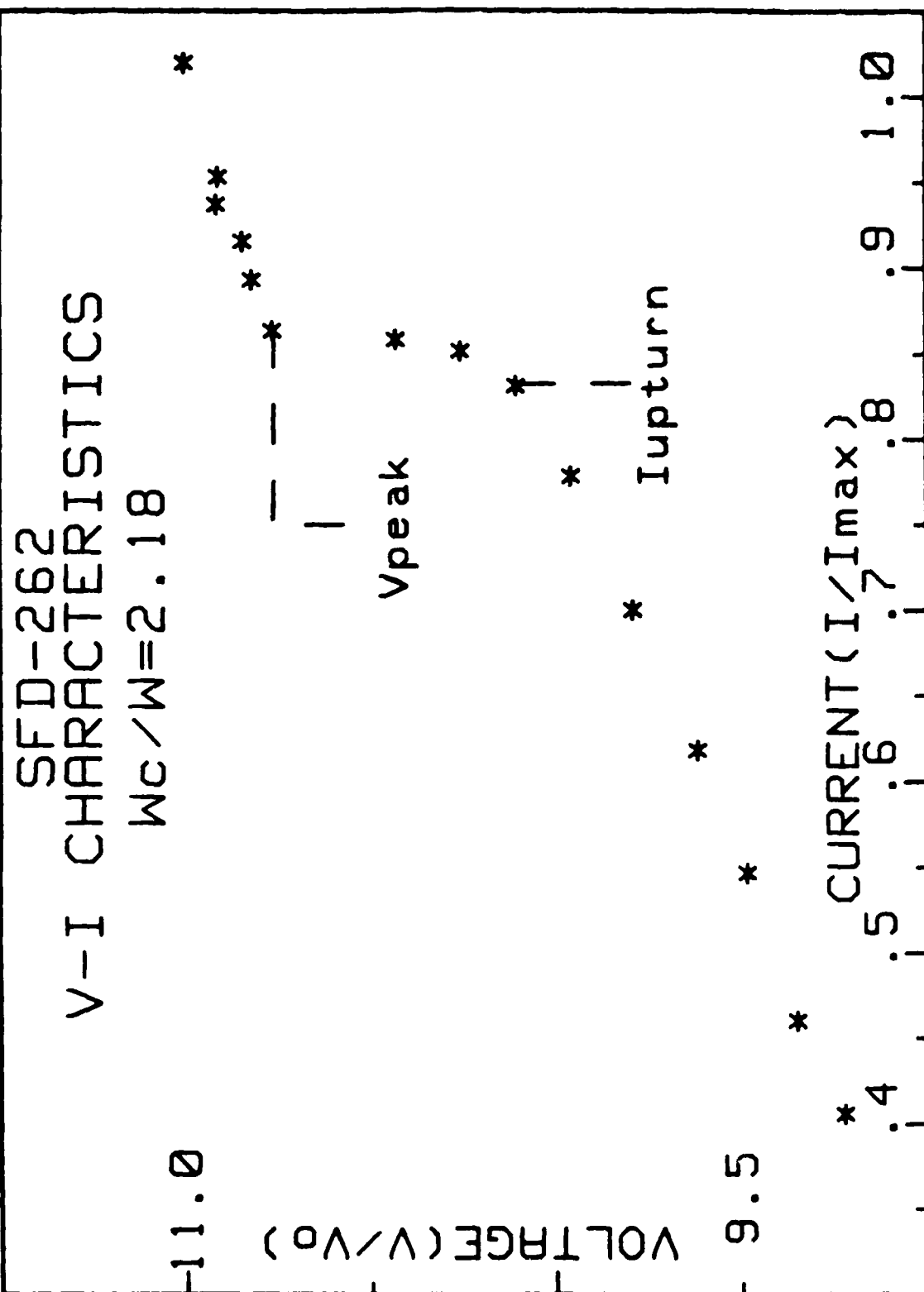


Fig. 12. V-I characteristics.

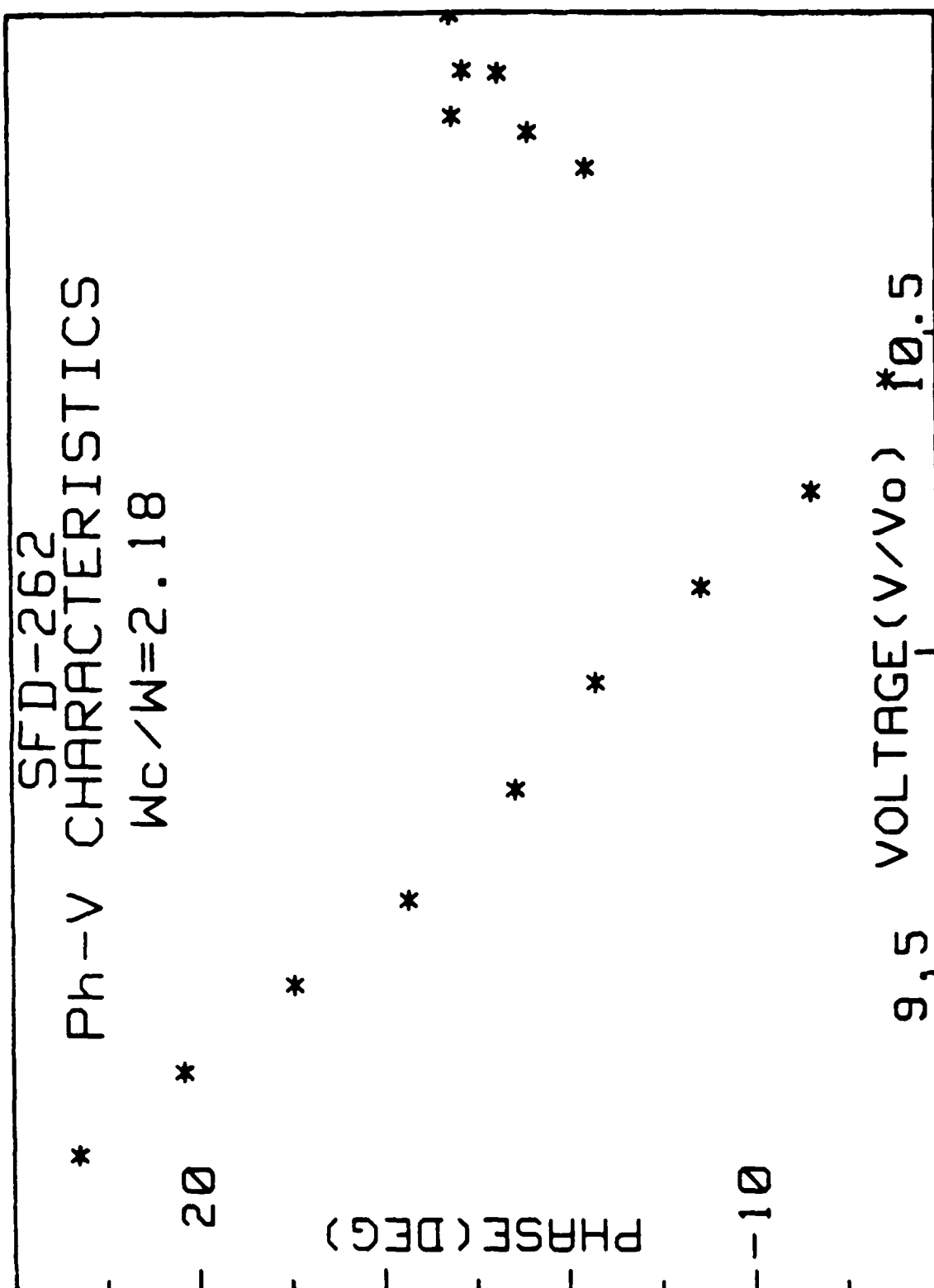


Fig. 13. Ph-V characteristics.

of the data points, error bars were generated to show the possible extent of these regime changes. These error bars are not shown in the examples just mentioned, so as not to unnecessarily clutter the picture being shown. However, error bars will be included in the overall experimental results to be presented.

Corresponding (but not the same) effects were found to be present in the V-I and Ph-V curves for the same magnetic field. These corresponding effects manifested themselves as characteristic changes in the current and phase parameters at the voltage positions of  $V_{\text{transition}}$  and  $V_{\text{roll over}}$  previously identified from the P-V curve. These corresponding changes were similarly characterized with error bars. Examples of these effects and error bars are again omitted to preserve the clarity of the curves presented in Figs. 12 and 13.

The net effect of the values generated from the three curves (P-V, V-I, Ph-V) was to reduce the error in determining the most probable voltages for both the transition and roll-over effects. This was accomplished by taking the intersection of the three individual values to form an overall experimental value with associated overall error bar. This value (but not the error bar) was recorded for each effect as a function of the 11 magnetic fields investigated and is given in Table 1.

Table 1. Experimentally determined regime voltages.

Normalized Magnetic Field ( $\omega_c/\omega$ )	Normalized Voltage ( $V/V_0$ )	
	$V_{\text{transition}}$	$V_{\text{roll over}}$
1.58	6.52	6.71
1.79	7.70	7.98
1.98	8.59	8.76
2.18	9.48	9.95
2.36	10.49	10.48
2.57	11.00	11.52
2.77	11.38	11.73
2.87	12.11	12.53
3.02	12.66	13.00
3.10	12.94	13.35
3.17	12.78	13.43

In addition, the current and voltage corresponding to an upturn ( $I_{\text{upturn}}$ ) and peak value ( $V_{\text{peak}}$ ), respectively, in the V-I curve were noted (see Fig. 12). In the case of the latter of these two effects, only 3 of the 11 possible values were able to be identified positively. The remaining 8 values were obscured because of excessive noise generation from the CFA. Lastly, the maximum power ( $P_{\text{max}}$ ) attainable in the mode of operation (see Fig. 11) was recorded as a function of magnetic field. The upturn current and maximum power values are tabulated in Table 2.



Table 2. Observed upturn current and maximum power values.

Normalized Parameters		
Magnetic Field ( $\omega_c/\omega$ )	Upturn Current ( $I/I_{\max}$ )	Maximum Power ( $P/P_0$ )
1.58	0.82	0.67
1.79	0.82	1.08
1.98	0.85	1.21
2.18	0.83	1.41
2.36	0.71	1.35
2.57	0.51	1.17
2.77	0.39	0.89
2.87	0.36	0.62
3.02	0.28	0.50
3.10	0.26	0.44
3.17	0.21	0.40

The previous figures and tables make use of the following normalizing parameters.  $V_0$  is a characteristic voltage value of classical crossed-field theory in which the Hull cutoff voltage equals the Hartree voltage.<sup>2</sup>  $I_{\max}$  is the theoretical peak current which is obtained from a soliton analysis of the CFA. This concept will not be addressed here, since it is beyond the scope of this paper.  $P_0$  is a defined power standard determined from the tube performance specification. Finally, the operating magnetic field value is normalized by the ratio of the cyclotron to operating frequency ( $\omega_c/\omega$ ), where the latter was a constant for this investigation. These normalizing factors will be used throughout the remainder of this report.

Having tabulated these regime transitions as a function of magnetic field, plots of these values were then made. These corresponding plots are shown in Figs. 14 through 16. For the sake of clarity in Fig. 14, exponential-like to linear transitions are denoted with a "\*", roll over points are given by a "+," and peak voltages are shown with a "#." In addition, error bars are included with these points to show the range of possible values for these voltages. However, the voltage scale required for this figure reduces these error bars to a diminutive size.

## 2. Theoretical Results

Theoretical results were obtained by using the relations governing the voltage regimes given by soliton theory, as presented in Chapter IV of this report. From these relations, curves were generated for the true synchronous voltage ( $V_{se}$ ), the soliton voltage ( $V_s$ ), and maximum operating voltage ( $V_{max}$ ) as a function of magnetic field. Additionally, the Hartree voltage ( $V_H$ ) curve was generated as a reference familiar to the tube community. These 4 curves have been incorporated into a single plot and are shown in Fig. 17.

Since the equations used in the generation of the theoretical curves required actual SFD-262 tube parameters, the actual derivations of these curves will not be shown in this paper. The tube parameters are proprietary information of Varian Associates.

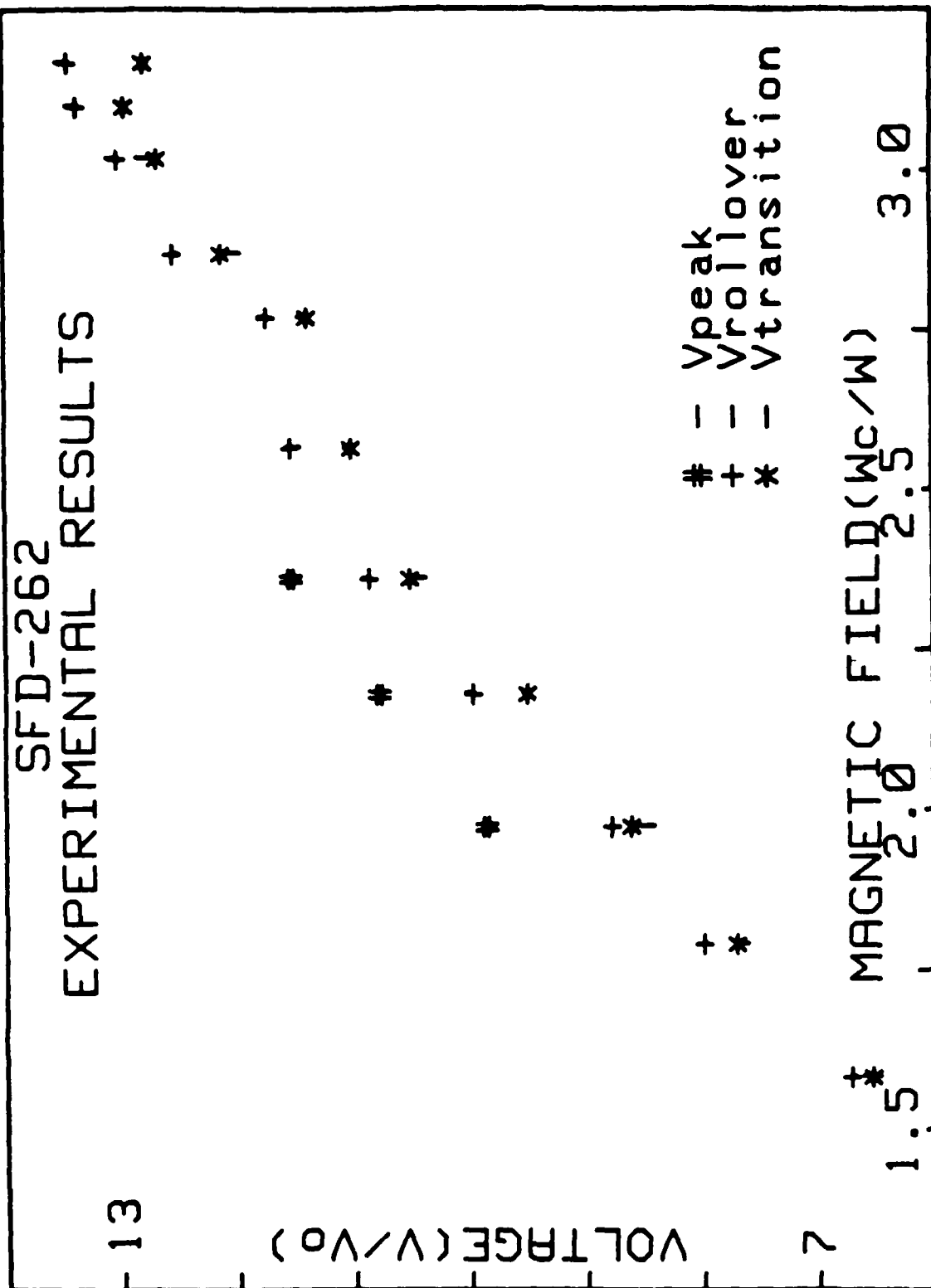


Fig. 14. Experimental results.

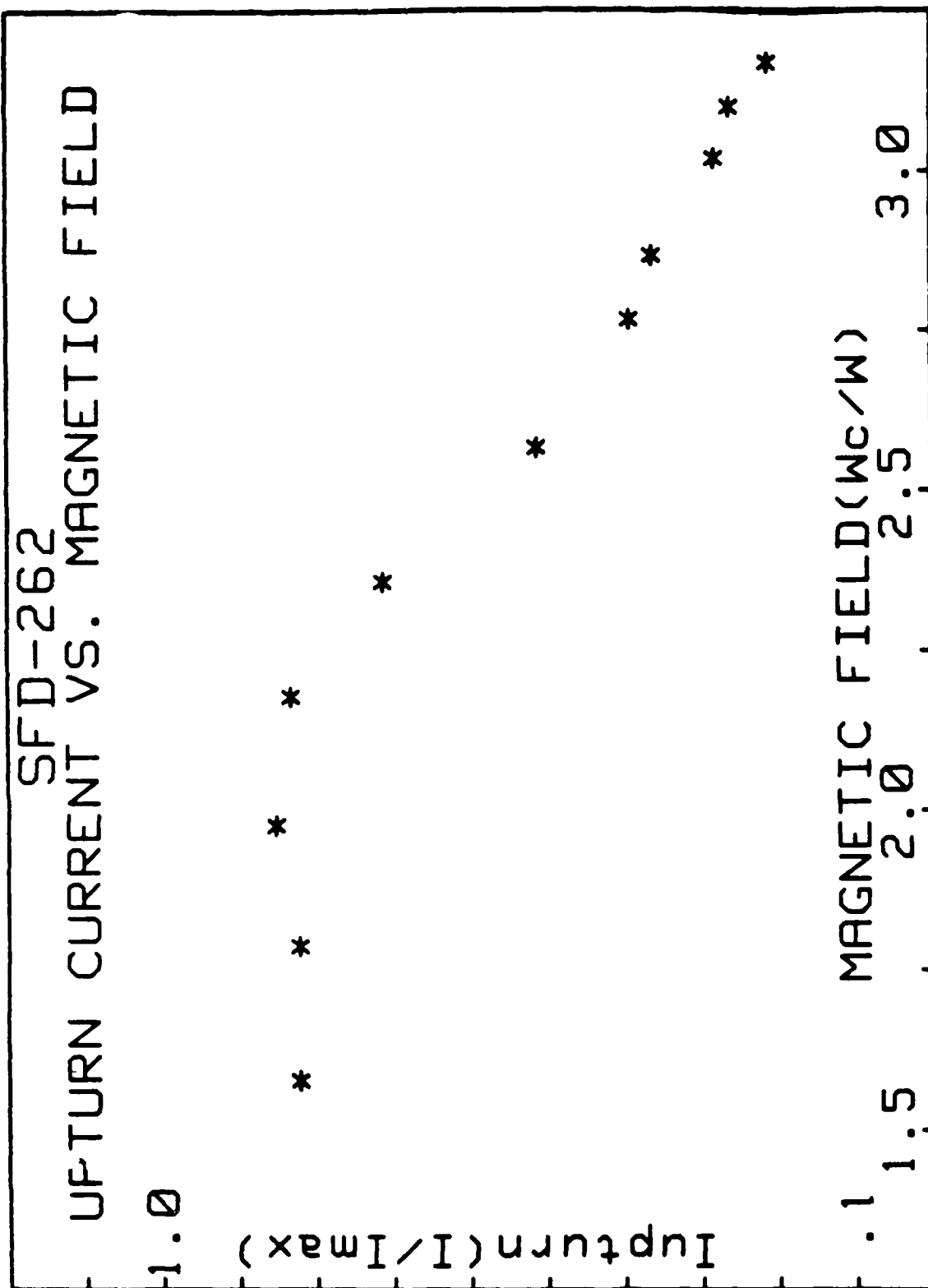


Fig. 15. Upturn current versus magnetic field.

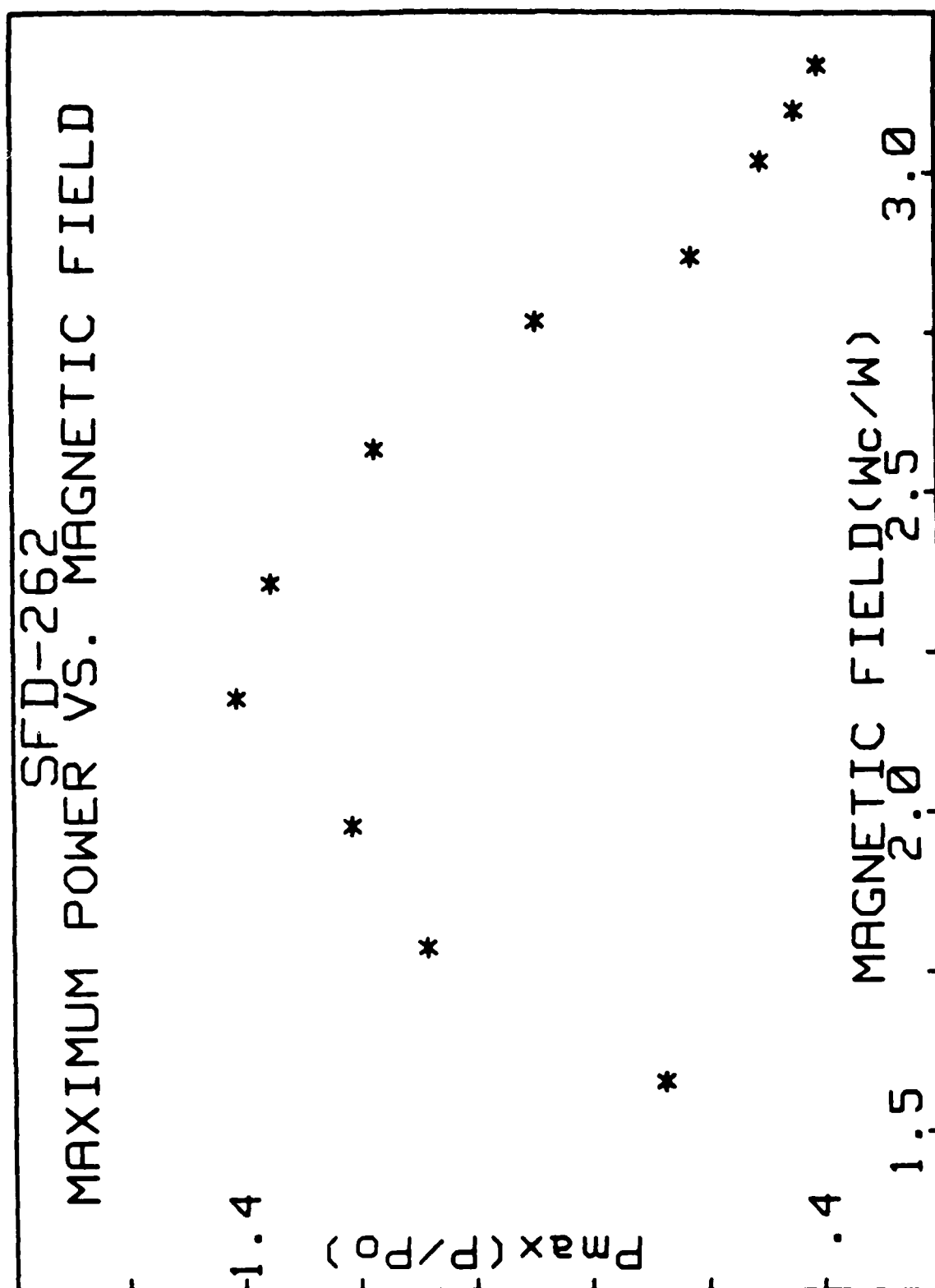


Fig. 16. Maximum power versus magnetic field.

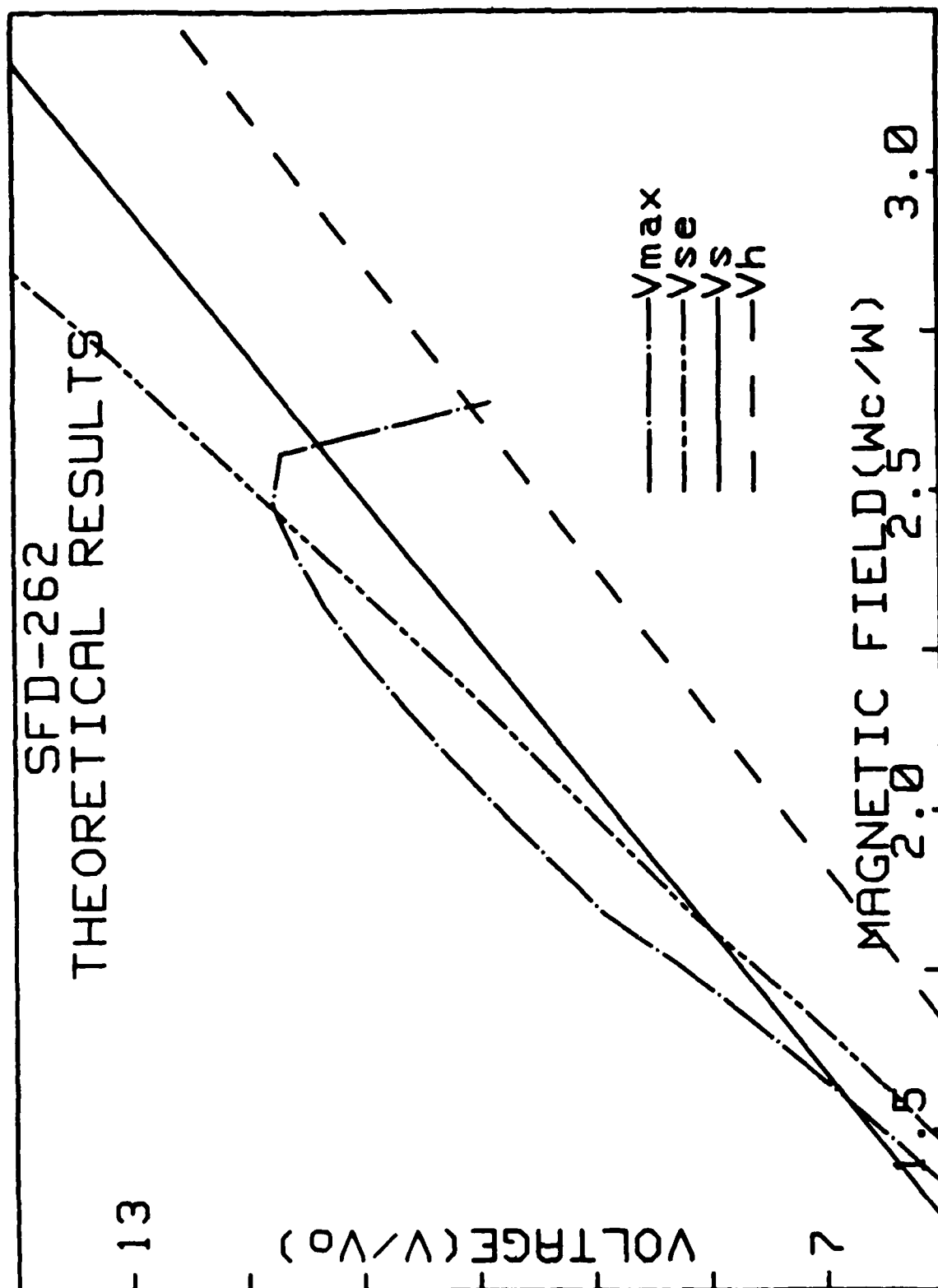


Fig. 17. Theoretical results.

## X. DISCUSSION AND COMPARISON OF RESULTS

Having completed both an experimental and theoretical treatment of the SFD-262, it is now the task to discuss and compare these two cases. This chapter will attempt to do this from a generic (CFAs in general) as well as a specific (SFD-262 CFA) point of view.

### 1. Discussion of Experimental Results

The data of Fig. 14 show a general trend in the regime voltages found by experimentation. In the low and mid-magnetic field regime ( $\omega_c/\omega < 2.4$ ), this trend is nearly linear. However, in the high magnetic regime ( $\omega_c/\omega > 2.4$ ), these voltages show a gradual slope decrease. This decrease seems to indicate a mechanism in the CFA which limits the operating voltages and currents in the high magnetic field regime. However, it is felt that the drastic decrease in regime voltages occurring at approximately  $\omega_c/\omega = 2.8$  are data points that are subject to question and are potentially in error. The source of this potential error is not known at this point. Similarly, it can be seen from Figs. 15 and 16 that this same limiting mechanism also affects both the available current and power in the high magnetic field regime.

In general, it can be said that CFA operating parameters initially increase as a function of magnetic field. However, after a specific point, a different parameter limiting regime is encountered. This change in operating characteristics defines the high magnetic field regime. The parameters affected by the limiting mechanism of this regime include the voltage, current, and consequently output power. In

addition to the above effects, CFA operation becomes progressively noisier, thereby to some degree obscuring these parameters.

## 2. Discussion of Theoretical Results

Turning to the theoretical results, the curves associated with Fig. 17 show a number of characteristics. First, at very low magnetic field values ( $\omega_c/\omega < 1.8$ ), the soliton voltage ( $V_s$ ) is greater than the true synchronous voltage ( $V_{se}$ ). At  $\omega_c/\omega = 1.8$ , there is a discontinuous crossing of these curves. From this point on, they continue in a linear diverging manner. Superimposed on these values is the maximum voltage ( $V_{max}$ ) curve. It initially has a value between  $V_{se}$  and  $V_s$ , but then quickly rises well above the other two curves. At approximately  $\omega_c/\omega = 2.5$ ,  $V_{max}$  once again crosses  $V_s$  and  $V_{se}$  and then falls off rather rapidly until encountering the Hartree voltage ( $V_H$ ) curve. It is not clear at this point what trend the  $V_{max}$  curve then assumes. This is an area of continuing theoretical investigation.

The significance of these theoretical curves is that they form a defining set of CFA characteristics based on the concepts presented in Chapter IV of this work.  $V_{se}$  and  $V_s$  define a set of CFA operating characteristics as a function of magnetic field. Additionally, the role of the  $V_{max}$  curve is to set an upper limit to the allowable operating voltage irrespective of the values of  $V_s$  and  $V_{se}$ . In other words, if  $V_{max}$  is less than  $V_{se}$  and  $V_s$ , then the values associated with these latter regimes will not be realized, since  $V_{max}$  will assume a limiting role. Conversely, if  $V_{max}$  is greater than these regime values, then  $V_{se}$  and  $V_s$  will indeed exist along with  $V_{max}$ .



These effects are shown by considering Fig. 17 once again.  $V_{\max}$  is greater than  $V_s$  and  $V_{se}$  in the magnetic field range of  $1.6 < \omega_c/\omega < 2.4$  and therefore would not limit values associated with these regimes. On the other hand, for the range of magnetic fields such that  $\omega_c/\omega < 1.6$  or  $\omega_c/\omega > 2.4$ ,  $V_{\max}$  is a limiting factor, since its value is lower than  $V_{se}$  and/or  $V_s$ , as the case may be. Its net effect is to modify the expected CFA behavior in those magnetic field regimes. As a result,  $V_{\max}$  is postulated to be responsible for the saturation mechanism known to be present in CFAs operating at high operating magnetic fields.

By virtue of the  $V_{\max}$  curve, the expected behavior of the CFA in the saturation regime is a decrease in the maximum attainable operating parameters there. These parameters include the CFA operating current and RF power output. The decrease in current is thought to be due to a competitive bunching mechanism present in the interaction area that limits the number of electrons available when operating in the saturation regime. Since CFA RF power output is heavily dependent on available current, a decrease in power would be an expected byproduct. The effects of the competitive bunching mechanism is more pronounced at the high magnetic field values, since competitive bunching is directly related to the size of the electron orbit.

### 3. Comparison Between Experimental and Theoretical Results

A direct comparison of results is made by superimposing Figs. 17 and 14. This resulting composite graph is shown in Fig. 18. In general, this comparison shows agreement over a wide range of magnetic

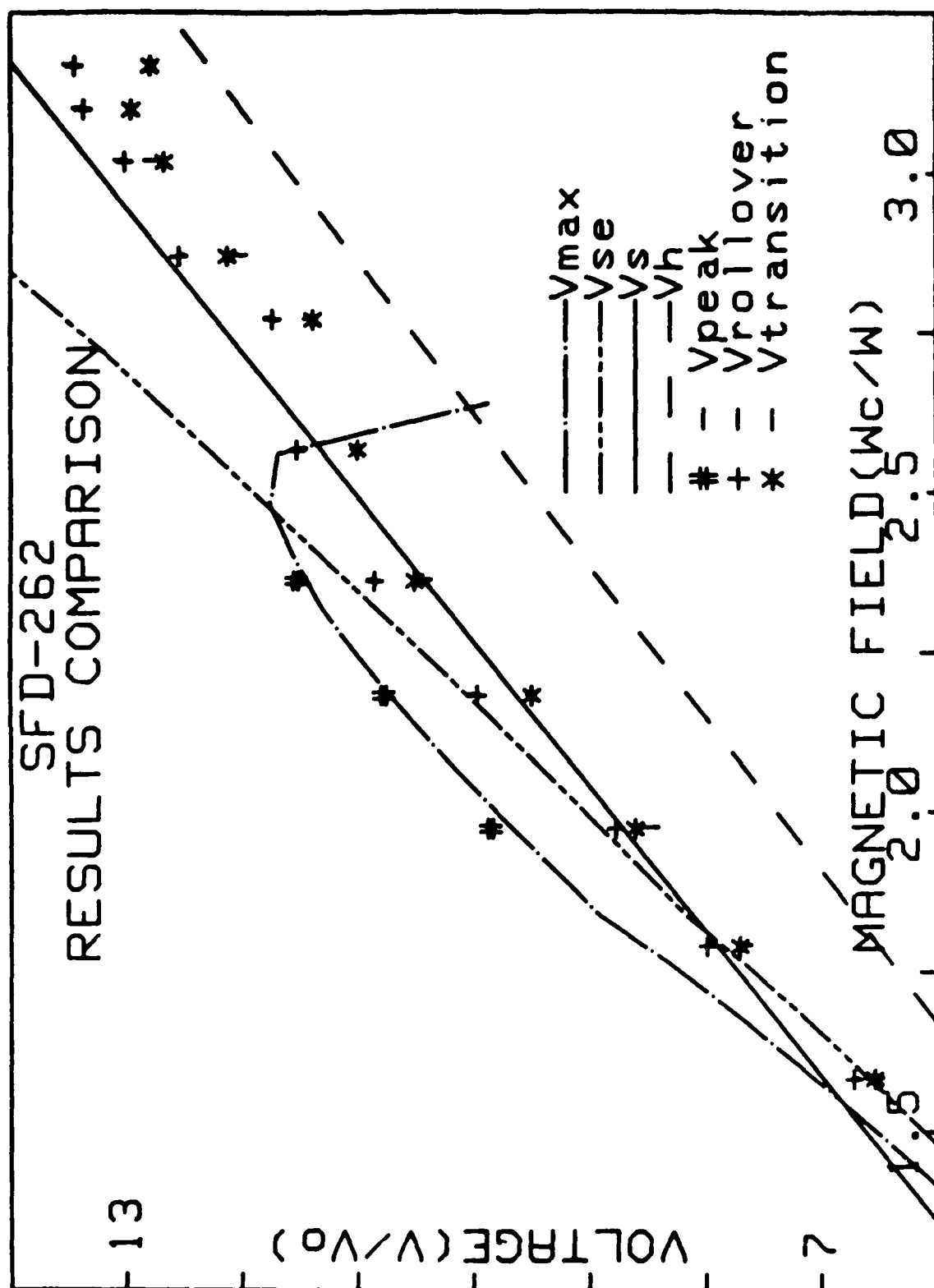


Fig. 18. Results comparison.

fields values. However, there are some portions of the comparison where irregularities arise.

Considering comparison in the mid-magnetic field regime first, one finds that the experimental data points and theoretical curves follow each other rather well. This occurs in the magnetic field range of  $1.8 < \omega_c/\omega < 2.4$ , where there is a near identity between  $V_{se}$  and  $V_s$  and the transition and roll-over voltages. It can be seen in this range that  $V_s$  corresponds to the transition points and  $V_{se}$  corresponds to the roll-over points. In addition, there is also excellent correlation between the values corresponding to  $V_{peak}$  and the  $V_{max}$  curve in this regime. More data will be required to completely characterize this equality.

In the low magnetic field regime ( $\omega_c/\omega < 1.8$ ), the agreement is almost as good. As described in the last section, the  $V_{max}$  curve has the effect of limiting the operating voltages expected in this regime. This is witnessed by the depressed value for the roll-over voltage when compared to the  $V_s$  curve at  $\omega_c/\omega = 1.58$ . Again, more data points are needed in this regime before a generalization of this effect can be made. Based on the tracking of the data points with the theoretical curves in this regime, it is evident that  $V_{se}$  corresponds to the transition point, while  $V_s$  assumes the roll-over point characteristic. This is a role reversal of the high and mid-magnetic field characteristics.

In the high magnetic field regime ( $\omega_c/\omega > 2.4$ ), the exactness of the agreement breaks down, although general characteristics have been preserved. Although values for  $V_{peak}$  are not available here, the data points shown give a picture of a saturation effect described by  $V_{max}$ . The data presented for  $V_{se}$  and  $V_s$  show a saturation effect occurring

at  $\omega_c/\omega \approx 2.4$  and greater, becoming more pronounced as the magnetic field is increased. The theory (through  $V_{\max}$ ) predicts that this effect occurs in a more drastic fashion, eventually lowering the voltages to  $V_H$ . The fact that the tube is operating at voltages above this theoretical value suggests that a correction for the  $V_{\max}$  curve is needed. A valid correction would cause this saturation effect to manifest itself in a less pronounced way as the data seem to indicate.

## XI. CONCLUSIONS AND FUTURE WORK

The results of a soliton analysis of the SFD-262 CFA have shown a promising amount of success when compared to data from actual tube operation. Soliton theory has correctly predicted device operation over a wide range of parameter space, but needs to resolve irregularities that exist over other areas of comparison.

The importance of these accomplishments is three-fold. First, it has given credence to a rigorous analytic treatment of a microwave device whose past understanding was based on an empirical knowledge of tube operation. Second, the irregularities encountered will pave the way for future theoretical work concerning microwave CFA modeling. Hopefully, a greater understanding of tube operation will result from this future work. Last, it has established a data base that will be used as a reference by other experiments done with SFD-262 CFAs or other CFAs.

The goal of future work is to extend the efforts presented here. This will be done from a number of avenues. Additional experiments will be conducted to establish a data base for the purpose of comparison to soliton based theory. Special concentration will be directed toward obtaining data at both the extremely low and high magnetic field regimes where other interactions may exist. A complete characterization of CFA behavior will result from this work. The latter regime will require an upgrade of the present SFD-262 modulator to obtain the voltages required at high magnetic field values. In addition, interim computing and automating upgrades will be made so that accuracy in data collection and

storage can be improved. Last, a voltage controllable version of the SFD-262 is being investigated as a test vehicle. This tube would feature a control electrode and thus would hopefully eliminate the problems of mode competition associated with the present constant current SFD-262.

## REFERENCES

1. G. B. Collins, Ed., *Microwave Magnetrons*, MIT Radiation Laboratory Series, McGraw-Hill Book Company, New York, Vol. 6, 1948.
2. J. C. Slater, *Microwave Electronics*, D. Van Nostrand Company, New York, 1950.
3. E. Okress, Editor-in-Chief, *Crossed-Field Microwave Devices*, Vols. I and II, Academic Press, Inc., New York, 1961.
4. W. M. Bollen, B. Goplen, and G. E. Thomas, *Bulletin of the American Physics Society*, Vol. 28, No. 8, 1983, p. 1088.
5. A. Bers, "Linear Waves and Instabilities," *Plasma Physics*, Les Houches, 1972; Gordon and Breach Science Publishers, Inc., New York, 1975.
6. S. P. Yu, G. P. Kooyers, and O. Buneman, "Time Dependent Analysis of Electron-Wave Interaction in Cross-Fields," *Journal of Applied Physics*, Vol. 36, No. 8, 1965, p. 2550.
7. G. K. Farney and H. L. McDowell, "CFA Design Improvement Program," Final Report on Contract No. N00123-75-6-1294, Naval Ocean Systems Center, San Diego, California, June 1978.
8. G. E. Dombrowski and W. C. Price, "Analytic and Experimental Study of Reentrant Stream Crossed-Field Amplifiers," Report on Contract No. NAS-9710.
9. J. W. Poukey, *Bulletin of the American Physics Society*, Vol. 27, No. 8, 1982, p. 954.
10. A. T. Drobot, *International Electron Device Meeting Technical Digest*, Washington, DC, 1979.
11. G. E. Thomas, private communication.
12. G. E. Thomas, "A Nonlinear Theory for a Microwave Crossed-Field Amplifier," *International Electron Device Meeting Technical Digest*, December 1980, p. 176.
13. A. C. Scott, F. Y. F. Chu, and D. W. McLaughlin, "The Soliton: A New Concept in Applied Science," *Proceedings of the IEEE*, Vol. 61, No. 10, October 1973.
14. K. Lonngren and A. C. Scott, Eds., *Solitons in Action*, Academic Press, Inc., New York, 1978.

15. G. L. Lamb, *Elements of Soliton Theory*, John Wiley and Sons, New York, 1980.
16. A. R. Bishop, J. A. Krumhansl, and S. F. Trullinger, "Solitons in Condensed Matter: A Paradigm," *Physics Digest*, Vol. 1, 1980, p. 1.
17. J. Scott-Russell, "Report on Waves," *Report of the 14th Meeting of the British Association for the Advancement of Science*, John Murray, London, England, 1844, p. 311.
18. D. J. Korteweg and G. deVries, "On the Change of Form of Long Waves Advancing in a Rectangular Canal, and on a New Type of Long Stationary Waves," *Philos. Magazine*, Vol. 39, 1895, p. 422.
19. N. Krall and A. Trivelpiece, *Principles of Plasma Physics*, McGraw-Hill Book Company, New York, Chapters 7 and 8, 1973.
20. G. E. Thomas, "The Nonlinear Operation of a Microwave Crossed-Field Amplifier," *IEEE Transactions on Electron Devices*, Vol. ED-28, January 1981, p. 27.
21. F. Chen, *Introduction to Plasma Physics*, Plenum Press, New York, 1974, p. 256.
22. V. E. Sakharov, *Soviet Physics JETP* 35, 1972, p. 908.
23. A. Nayfeh, *Perturbation Methods*, John Wiley and Sons, New York, 1973.
24. M. Ablowitz and H. Segur, "On the Evolution of Packets of Water Waves," *Journal of Fluid Mechanics*, Vol. 92, Part 4, 1979, p. 691.
25. G. E. Thomas, "Soliton-Voltage and Phase Characteristics of Microwave Crossed-Field Amplifier," *IEEE Transactions on Electron Devices*, Vol. ED-29, August 1982, p. 1210.
26. G. E. Thomas, "Soliton Analysis of a Cross-Field Amplifier," Monthly Status Report on Contract No. N00164-82-C-0240, Naval Weapons Support Center, San Diego, California, February 1983.
27. Varian Associates, *Crossed-Field Amplifier, Klystron, and Magnetron Catalog*, No. 3345, Beverly, Massachusetts, 1975.



END

DTIC

8-86